



HAL
open science

The Autophagy Receptor TAX1BP1 (T6BP) improves antigen presentation by MHC-II molecules

Gabriela Sarango, Clémence Richetta, Mathias Pereira, Anita Kumari, Michael Ghosh, Lisa Bertrand, Cédric Pionneau, Morgane Le Gall, Sylvie Grégoire, Raphaël Jeger-Madiot, et al.

► To cite this version:

Gabriela Sarango, Clémence Richetta, Mathias Pereira, Anita Kumari, Michael Ghosh, et al.. The Autophagy Receptor TAX1BP1 (T6BP) improves antigen presentation by MHC-II molecules. *EMBO Reports*, 2022, 23 (12), 10.15252/embr.202255470 . hal-03864670

HAL Id: hal-03864670














<https://hal.science/hal-03864670v1>

Submitted on 21 Nov 2022

HAL is a multi-disciplinary open access archive for the deposit and dissemination of scientific research documents, whether they are published or not. The documents may come from teaching and research institutions in France or abroad, or from public or private research centers.

L'archive ouverte pluridisciplinaire **HAL**, est destinée au dépôt et à la diffusion de documents scientifiques de niveau recherche, publiés ou non, émanant des établissements d'enseignement et de recherche français ou étrangers, des laboratoires publics ou privés.

The Autophagy Receptor TAX1BP1 (T6BP) improves antigen presentation by MHC-II molecules

Gabriela Sarango^{1,2,†} , Clémence Richetta^{2,3,†}, Mathias Pereira^{1,2,†} , Anita Kumari^{1,2} , Michael Ghosh⁴ , Lisa Bertrand^{1,2} , Cédric Pionneau⁵ , Morgane Le Gall⁶ , Sylvie Grégoire^{1,2}, Raphaël Jeger-Madiot^{2,‡}, Elina Rosoy², Frédéric Subra³, Olivier Delelis³, Mathias Faure^{7,8} , Audrey Esclatine¹, Stéphanie Graff-Dubois^{2,‡} , Stefan Stevanović⁴ , Bénédicte Manoury^{9,*} , Bertha Cecilia Ramirez^{1,2}  & Arnaud Moris^{1,2,**} 

Abstract

CD4⁺ T lymphocytes play a major role in the establishment and maintenance of immunity. They are activated by antigenic peptides derived from extracellular or newly synthesized (endogenous) proteins presented by the MHC-II molecules. The pathways leading to endogenous MHC-II presentation remain poorly characterized. We demonstrate here that the autophagy receptor, T6BP, influences both autophagy-dependent and -independent endogenous presentation of HIV- and HCMV-derived peptides. By studying the immunopeptidome of MHC-II molecules, we show that T6BP affects both the quantity and quality of peptides presented. T6BP silencing induces the mislocalization of the MHC-II-loading compartments and rapid degradation of the invariant chain (CD74) without altering the expression and internalization kinetics of MHC-II molecules. Defining the interactome of T6BP, we identify calnexin as a T6BP partner. We show that the calnexin cytosolic tail is required for this interaction. Remarkably, calnexin silencing replicates the functional consequences of T6BP silencing: decreased CD4⁺ T cell activation and exacerbated CD74 degradation. Altogether, we unravel T6BP as a key player of the MHC-II-restricted endogenous presentation pathway, and we propose one potential mechanism of action.

Keywords calnexin; CD4⁺ T cell activation; interactome; immunopeptidome; virus

Subject Categories Autophagy & Cell Death; Immunology; Signal Transduction

DOI 10.15252/embr.202255470 | Received 23 May 2022 | Revised 16 September 2022 | Accepted 23 September 2022

EMBO Reports (2022) e55470

Introduction

CD4⁺ helper T cells that orchestrate adaptive immune responses recognize pathogen- or tumor-derived peptides presented by the major histocompatibility complex class II (MHC-II) molecules. MHC-II molecules are expressed by professional antigen-presenting cells (APC) such as B cells, macrophages and dendritic cells (DC), thymic epithelial cells (TEC), and by nonprofessional APCs in inflammatory conditions (Roche & Furuta, 2015; Wijdeven *et al*, 2018). The MHC-II transactivator, CIITA, governs the transcription of the MHC-II locus that includes genes encoding for the α - and β -chains of MHC-II molecules, the invariant chain (called Ii or CD74), and the chaperon proteins HLA-DM/HLA-DO (Reith *et al*, 2005). The transmembrane α - and β -chains are assembled within the endoplasmic reticulum (ER), where they associate with CD74 leading to the formation of nonameric $\alpha\beta$ -CD74 complexes that traffic into late endo-lysosomal compartments named MIIC (Bakke & Dobberstein, 1990; Lotteau *et al*, 1990; Neefjes *et al*, 1990; Roche *et al*, 1991). In the MIIC, CD74 is progressively cleaved by vesicular proteases (Riese *et al*, 1996; Nakagawa *et al*, 1998; Shi *et al*, 2000; Manoury

1 Université Paris-Saclay, CEA, CNRS, Institute for Integrative Biology of the Cell (I2BC), Gif-sur-Yvette, France

2 Sorbonne Université, INSERM, CNRS, Center for Immunology and Microbial Infections (CIMI-Paris), Paris, France

3 LBPA, ENS-Paris Saclay, CNRS UMR8113, Université Paris Saclay, Gif-sur-Yvette, France

4 Department of Immunology, Institute for Cell Biology, University of Tübingen, Tübingen, Germany

5 Sorbonne Université, INSERM, UMS Production et Analyse de Données en Sciences de la vie et en Santé, PASS, Plateforme Post-génomique de la Pitié Salpêtrière, Paris, France

6 3P5 proteom¹C facility, Université de Paris, Institut Cochin, INSERM U1016, CNRS-UMR 8104, Paris, France

7 CIRI, Centre International de Recherche en Infectiologie, Université de Lyon, Inserm U1111, Université Claude Bernard Lyon 1, CNRS, UMR5308, ENS de Lyon, Lyon, France

8 Equipe Labellisée par la Fondation pour la Recherche Médicale, FRM

9 Institut Necker Enfants Malades, INSERM U1151-CNRS UMR 8253, Faculté de médecine Necker, Université de Paris, Paris, France

*Corresponding author. Tel: +33 140615382; E-mail: benedicte.manoury@inserm.fr

**Corresponding author. Tel: +33 169826294; E-mail: arnaud.moris@i2bc.paris-saclay.fr

†These authors contributed equally to this work

‡Present address: Sorbonne Université, INSERM U959, Immunology-Immunopathology-Immunotherapy (i3), Paris, France

et al, 2003), leaving a residual MHC-II-associated Ii peptide (CLIP) that occupies the peptide binding groove (Roche & Cresswell, 1991; Bijlmakers et al, 1994; Busch et al, 1996). HLA-DM then facilitates the exchange of the CLIP fragments with high-affinity peptides generated from pathogen- or tumor-derived antigens (Morris et al, 1994; Sanderson et al, 1994; Denzin & Cresswell, 1995). MHC-II molecules are then transported to the plasma membrane to expose antigenic peptides to CD4⁺ T cells (Thibodeau et al, 2019).

MHC-II molecules present peptides derived from extra- and intracellular sources of antigens, so-called exogenous and endogenous presentation, respectively (Watts, 2004; Veerappan Ganesan & Eisenlohr, 2017). Extracellular antigens are captured and internalized into APCs by various means including macropinocytosis, phagocytosis, or receptor-mediated endocytosis (Roche & Furuta, 2015). Antigens are then delivered to the MIIC where they are progressively degraded by endo-lysosomal proteases such as cathepsins (Watts, 2004), into peptides (or epitopes) ranging from 12 to 25 amino acids in length, that can be loaded on nascent MHC-II molecules (Rudensky et al, 1991; Unanue et al, 2016). Epitopes from extracellular antigens can also bind, in early endosomes, to recycling MHC-II molecules (Pinet et al, 1995; Sinnathamby & Eisenlohr, 2003). The endogenous pathway relies on protein antigen synthesis by virus-infected (Jacobson et al, 1988; Sekaly et al, 1988; Eisenlohr & Hackett, 1989; Jaraquemada et al, 1990; Nuchtern et al, 1990; Thiele et al, 2015) or tumor cells (Tsuji et al, 2012). Some early *in vitro* studies showed that neosynthesized self-epitopes are displayed, after lysosomal proteolysis, by MHC-II molecules leading to CD4⁺ T cell activation (Bikoff & Birshstein, 1986; Rudensky & Yurin, 1989; Weiss & Bogen, 1989). More recently, it was shown that the initiation of CD4⁺ T cell responses to *influenza virus* is mainly driven by epitopes derived from the processing of intracellular antigens within APCs (Miller et al, 2015). However, the pathways leading to the loading of MHC-II molecules with endogenous antigens remain poorly characterized. Components of the MHC class I (MHC-I) processing pathway such as proteasome have been implicated (Lich et al, 2000; Tewari et al, 2005). One unresolved issue is how cytosolic antigens are transported into MHC-II-enriched compartments (Dani et al, 2004; Crotzer & Blum, 2008). For some specific epitopes but not others, the transporter associated with antigen presentation of MHC-I molecules (TAP) has been linked with the delivery of endogenous peptides on MHC-II molecules (Malnati et al, 1992; Tewari et al, 2005). In fact, depending on the cellular localization, the trafficking, and the nature of the antigen itself, different pathways might be involved in the degradation and delivery of endogenous antigens to MHC-II loading compartments (Mukherjee et al, 2001; Tewari et al, 2005; Leung, 2015).

The pathways of autophagy contribute to the processing of MHC-II-restricted endogenous antigens. The receptor of chaperone-mediated autophagy, LAMP-2A, has been shown to facilitate the presentation of a cytosolic self-antigen by MHC-II molecules (Zhou et al, 2005). The analysis of the MHC-II immunopeptidome revealed that macroautophagy (herein referred to as autophagy) also contributes to the processing of cytoplasmic and nuclear antigens (Dengiel et al, 2005). Autophagy is a self-eating cellular degradation pathway, in which double-membrane autophagosomes deliver their cytoplasmic constituents for lysosomal degradation (Kirkin, 2020). Using various models, several labs established that autophagy

participates, in TECs, in the generation of MHC-II-restricted endogenous epitopes and strongly influences the thymic selection of autoreactive CD4⁺ T cells (Aichinger et al, 2013; Schuster et al, 2015). Other evidence that autophagy plays a role in endogenous antigen presentation comes from *in vitro* studies using APCs transfected with mRNAs encoding tumor antigens (Dorfel et al, 2005) or cDNAs encoding tumor or viral antigens targeted to autophagosomes (Schmid et al, 2007; Jin et al, 2014; Coulon et al, 2016; Fonteneau et al, 2016). Targeting antigens to autophagosomes through the fusion to LC3, an autophagy effector that incorporates into and participates in the elongation of autophagosomes enhances the capacity of APCs to activate antigen-specific CD4⁺ T cells (Coulon et al, 2016). However, overall, there are few examples where endogenous degradation of native tumors or viral antigens has been shown to be dependent on autophagy (Paludan et al, 2005; Leung, 2015). In fact, autophagy effectors may directly or indirectly affect the presentation of MHC-II-restricted antigens (Fletcher et al, 2018) by regulating, for instance, the delivery of proteases into the MIIC (Lee et al, 2010). Thereafter, autophagy also contributes to the exogenous presentation of viral and bacterial antigens (Jagannath et al, 2009; Blanchet et al, 2010). The molecular links between autophagy and MHC-II-restricted antigen presentation, in particular the mechanisms allowing the delivery of autophagy-degraded antigens to the MIIC, are poorly defined.

A growing body of evidence indicates that autophagosomes selectively target their cargos while excluding the rest of the cytoplasmic content (Kirkin, 2020). Several forms of selective autophagy exist, depending on the substrate, but all rely on the so-called autophagy receptors (ARs) that include: Nuclear Dot Protein 52 (NDP52), Optineurin (OPTN), Sequestosome-1 / p62, Next to BRCA1 gene protein-1 (NBR1) and TAX1-binding protein-1 also called TRAF6-binding protein (TAX1BP1/T6BP) (Kirkin & Rogov, 2019). ARs contain ubiquitin (Ub) and LC3-binding domains that allow, on the one hand, binding to ubiquitinated proteins and, on the other hand, their targeting into autophagosomes through interaction with LC3 on the internal membranes of forming autophagosomes (Kirkin & Rogov, 2019). As such, ARs are involved in multiple cellular processes including selective degradation of incoming bacteria and of damaged mitochondria, processes called xenophagy (Tumbarello et al, 2015) and mitophagy (Randow & Youle, 2014), respectively. In addition to their role in selective autophagy, T6BP, NDP52, and OPTN are required for the maturation of autophagosomes (Tumbarello et al, 2012). Thanks to the binding to myosin-VI, these ARs bridge autophagosomes to Tom-1-expressing endosomes and lysosomes, thus facilitating their fusion (Sahlender et al, 2005; Morriswood et al, 2007; Tumbarello et al, 2012). T6BP, OPTN, and NDP52, by promoting autophagosome maturation (Verlhac et al, 2015), are essential for the degradation of *Salmonella typhimurium* (Thurston et al, 2009; Wild et al, 2011; Lin et al, 2019). Remarkably, T6BP, NDP52, and p62 were also shown to orchestrate the maturation of early endosomes into late endosomes (Jongsma et al, 2016). This process also involves the Ub-binding domain of these receptors (Jongsma et al, 2016). Therefore, ARs exert multiple redundant but also exclusive roles in selective autophagy and in the traffic and maturation of vesicles such as autophagosomes and endosomes.

Here, we hypothesize that ARs may contribute at various, so far unknown, levels to MHC-II-restricted viral antigen presentation. We

show that silencing of NDP52, OPTN, and p62 in model APCs does not significantly affect the presentation of an autophagy-dependent antigen to CD4⁺ T cells. By contrast, T6BP influences both autophagy-dependent and -independent endogenous viral, as well as cellular, antigen processing and presentation by MHC-II molecules. In fact, the action of T6BP is not limited to viral antigens since the global repertoire of peptides presented by MHC-II molecules (immunopeptidome) is dramatically changed upon T6BP silencing. We show that T6BP silencing does not perturb the global cell-surface expression nor internalization kinetics of MHC-II molecules. However, it induces significant relocalization of the MIIC closer to the nucleus and the generation of unstable MHC-II-peptide complexes. Importantly, we demonstrate that the absence of T6BP expression induces a strong and rapid degradation of the invariant chain CD74, which directly influences the quality of the peptide repertoire loaded on MHC-II molecules. Finally, to get a hint on possible mechanisms, we defined the interactome of T6BP and identified novel protein partners that potentially participate in the T6BP-mediated regulation of the MHC-II peptide loading process. Among them, we identified the ER chaperone calnexin (CANX). We show that T6BP binds the cytoplasmic tail of CANX known to regulate its ER functions. Finally, we provide the direct demonstration that silencing CANX also induces CD74 degradation and decreases the capacity of model APCs to activate CD4⁺ T cells. Altogether, this study unravels a new role for T6BP as a key player in MHC-II-restricted antigen presentation, and in CD4⁺ T cell immunity.

Results

T6BP silencing influences endogenous viral antigen presentation and CD4⁺ T cell activation

Owing to their functions in selective autophagy and in the maturation of autophagosomes, we focused our work on NDP52, OPTN, and T6BP asking whether these ARs might be involved in endogenous antigen presentation by MHC-II molecules and subsequent activation of CD4⁺ T cells. To this end, HeLa cells modified to express CIITA (HeLa-CIITA) were silenced for the expression of ARs using siRNAs targeting NDP52, OPTN, and T6BP and evaluated for their capacity to activate CD4⁺ T cell clones (Fig 1A). An siRNA targeting p62 was also included as this AR plays, in multiple models, a dominant role in selective autophagy but does not participate in the maturation of autophagosomes (Tumbarello *et al*, 2012). 24 h post-siRNA transfection HeLa-CIITA cells were transfected with a plasmid encoding HIV Gag protein fused to LC3. This Gag-LC3 fusion enables specific targeting of Gag into autophagosomes and enhances HIV-specific T cell activation in an autophagy-dependent manner (Coulon *et al*, 2016). 48 h post-siRNA treatment (24 h post-DNA transfection), we analyzed by flow cytometry the percentages of living and of Gag-positive (Gag⁺) cells, using viability dye and Gag intracellular staining, respectively (Appendix Fig S1A). In all tested conditions, the levels of Gag⁺ cells were similar and the sequential transfections (siRNA and cDNA) had no significant influence on cell viability (Appendix Fig S1B and C). The silencing of AR expression was also analyzed by Western Blot (WB). As compared to the control siRNA (CTRL), all siRNAs led to a marked decrease in AR expression (Fig 1B). HeLa-CIITA cells were then co-cultured with

Gag-specific CD4⁺ T cells that we previously isolated and characterized (Moris *et al*, 2006). These Gag-specific CD4⁺ T cell clones recognize HIV-infected cells (Moris *et al*, 2006; Coulon *et al*, 2016). CD4⁺ T cell activation was monitored using IFN γ -ELISPOT (Fig 1C). Cells transfected with CTRL, NDP52, OPTN, or p62 targeting siRNAs led to similar levels of CD4⁺ T cell activation (Fig 1C, right and left panel). By contrast, T6BP silencing greatly decreased the activation of Gag-specific T cells (Fig 1C, left panel). On average, T6BP silencing led to a 75% decrease in Gag-specific CD4⁺ T cell activation (Fig 1C, right panel).

We next analyzed the effect of T6BP silencing on autophagy-independent endogenous viral antigen processing and presentation by MHC-II molecules. As previously, HeLa-CIITA cells were first transfected with CTRL- or T6BP-targeting siRNAs (siCTRL and siT6BP, respectively), then transfected with various plasmids encoding Gag, Gag-LC3_{G120A}, or Gag-LC3, and co-cultured with the Gag-specific CD4⁺ T cells (Fig 1D). Importantly, in our previous work we demonstrated that newly synthesized Gag is processed in an autophagy-independent manner both in monocyte-derived DCs (MDDCs) and in HeLa-CIITA cells (Coulon *et al*, 2016). This was shown by using productively infected MDDCs and Gag-cDNA-transfected HeLa-CIITA cells treated with various drugs influencing autophagy (e.g., 3-MA, Spautin-1, and Torin-1), shRNA targeting LC3 or overexpressing a trans-dominant mutant of Atg4B (Atg4BC74A), which blocks the formation of autophagosomes. Using the same tools, we also showed that the fusion with LC3 (Gag-LC3) targets Gag to autophagosome-mediated degradation leading to an enhancement of CD4⁺ T cell activation. Gag-LC3_{G120A} was also used as a negative control for autophagy-dependent degradation, as the G120A mutation in the C-terminus of LC3 abolishes the lipidation and incorporation of LC3 in the nascent membranes of autophagosomes, thus preventing Gag targeting into autophagosomes. Finally, we showed that upon Gag-LC3_{G120A}-transfection, Gag antigens are processed in an autophagy-independent manner (Coulon *et al*, 2016). 24 h post-transfection and prior co-culture with the CD4⁺ T cells, the percentage of Gag⁺ cells, Gag expression levels and the cell viability were similar in all tested conditions (Appendix Fig S1C). As previously, T6BP silencing strongly decreased the capacity of HeLa-CIITA cells expressing Gag-LC3 to activate the Gag-specific T cells (Fig 1D, left panel). However, we observed that the effect of T6BP silencing was not limited to Gag-LC3 as the capacity of HeLa-CIITA expressing Gag- or Gag-LC3_{G120A} to activate the CD4⁺ T cell clones, was also reduced in siT6BP-treated cells (Fig 1D, left panel). Importantly, T6BP silencing did not interfere with the ability of HeLa-CIITA cells to present the cognate peptide recognized by Gag-specific T cells when the peptide was added exogenously (Fig 1D, right panel). These results suggest that T6BP silencing influences the generation of Gag-, Gag-LC3- and Gag-LC3_{G120A}-derived endogenous epitopes and their subsequent presentation by MHC-II molecules to Gag-specific CD4⁺ T cells but does not affect the presentation of exogenous peptides by MHC-II molecules. Note that we obtained similar results with several siRNAs targeting different exons and introns of T6BP mRNA. We then sought to extend these observations to additional viral antigens. To this end, HeLa-CIITA cells treated with siCTRL or siT6BP were transfected with a plasmid encoding the immunodominant pp65 HCMV antigen and co-cultured with a pp65-specific CD4⁺ T cell line (Fig 1A and E). Remarkably, T6BP silencing also led to a

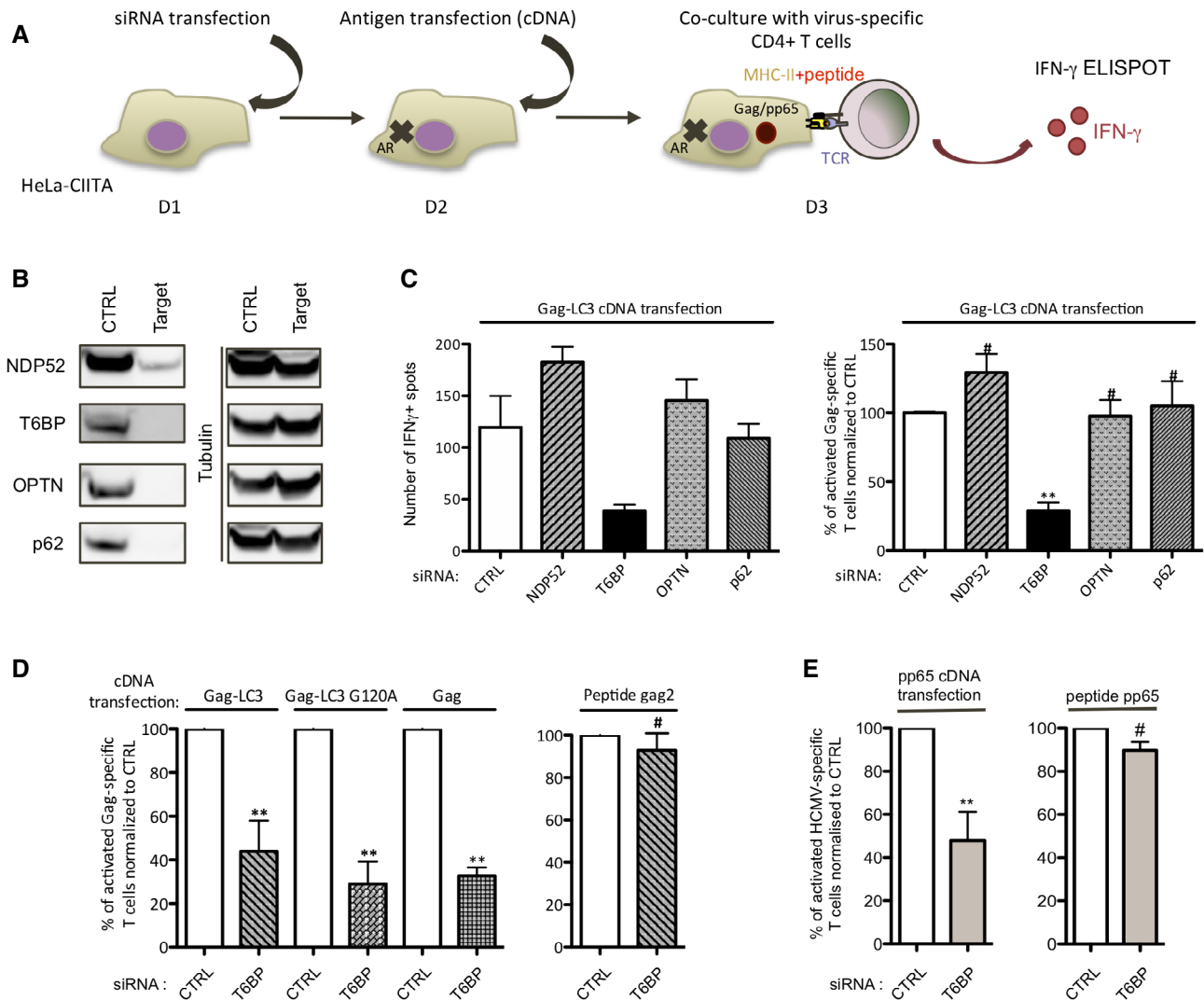


Figure 1. T6BP silencing decreases endogenous viral Ag presentation and CD4⁺ T cell activation.

- A** Schematic representation of the experiment. HeLa-CIITA cells were transfected with siRNAs targeting ARs and 24 h later with plasmids encoding the antigens: Gag, Gag-LC3, Gag-LC3 G120A, or pp65. 24 h post-DNA transfection, the HeLa-CIITA cells were co-cultured with antigen-specific CD4⁺ T cells and T cell activation was assessed using IFN- γ -ELISPOT. AR: Autophagy Receptor; D: day; TCR: T cell receptor.
- B** 48 h post-transfection of HeLa-CIITA cells with siRNAs targeting NDP52, T6BP, OPTN, and p62, AR expression was analyzed using Western Blot. Tubulin was used as control. The results are representative of at least 3 independent experiments and correspond to AR expression levels of the experiment in (C), left panel.
- C** Monitoring of Gag-specific CD4⁺ T cell activation. HeLa-CIITA cells were treated as indicated above and transfected with a plasmid encoding Gag-LC3. Left panel, a representative experiment is shown (\pm SD of three technical replicates). Right panel, three biological replicates are combined and presented as mean percentage (\pm SD). The y-axis represents the relative percentage of IFN- γ spots reported to the secretion of IFN- γ by the CD4⁺ T cell clones incubated with the siCTRL-treated HeLa-CIITA and set to 100%. The mean T cell activation levels of the three experiments using siCTRL or siT6BP were (100, 195, 119) and (35, 53, 38) IFN- γ ⁺ spots, respectively. 5,000 T cell clones were seeded per well in technical triplicates.
- D** Left panel, as in (C) right panel, but using DNA encoding Gag-LC3, Gag-LC3_{G120A}, or Gag. With Gag-LC3, Gag-LC3 G120A or Gag antigens, the mean T cell activation levels using siCTRL or siT6BP were (199, 435, 384), (91, 141, 119) and (343, 415, 385) or (98, 273, 171), (27, 50, 19) and (97, 148, 131) IFN- γ ⁺ spots, respectively. 5,000 T cell clones were seeded per well in technical triplicates. Three biological replicates are combined and presented as mean percentage (\pm SD). Right panel, influence of T6BP silencing on peptide presentation by HeLa-CIITA cells. The cognate peptide was added exogenously (gag2, 0.1 μ g/mL) on siRNA-treated cells (2 h, 37°C), washed and T cell activation monitored using IFN- γ -ELISPOT. The mean T cell activation levels using siCTRL or siT6BP were (100, 45, 42) and (71, 45, 33) IFN- γ ⁺ spots, respectively. 1,000 T cell clones were seeded per well in technical triplicates. Three biological replicates are combined and presented as mean percentage (\pm SD).
- E** As in (D) but using cDNA encoding HCMV pp65 antigen (left panel) or pp65 peptide (0.5 μ g/mL; right panel) and a pp65-specific CD4⁺ T cell line. Results of three independent experiments are represented. The mean T cell activation levels using siCTRL or siT6BP and pp65 DNA were (66, 106, 99) and (39, 50, 33) IFN- γ ⁺ spots, respectively. For the peptide: siCTRL or siT6BP: (185, 317, 415) and (163, 292, 381) IFN- γ ⁺ spots, respectively. 1,000 or 2000 T cell clones were seeded per well in technical triplicates.

Data information: For all ELISPOT experiments, the background secretions of IFN- γ by CD4⁺ T cells co-cultured with mock-treated HeLa-CIITA cells were used as negative controls and subtracted. CTRL—control. Wilcoxon's test; the symbols correspond to ** $p < 0.01$ and # $p > 0.05$ comparing each experimental conditions solely with its internal control (siCTRL).

Source data are available online for this figure.

strong reduction in CD4⁺ T cell activation (Fig 1E, left panel). As previously, the capacity of HeLa-CIITA cells to present the cognate pp65-derived peptide, added exogenously, was not affected (Fig 1E, right panel). These results demonstrate that regardless of the antigen tested, T6BP silencing dramatically influences the capacity of APCs to activate antigen-specific CD4⁺ T cells. The effect of T6BP silencing is broader than we initially anticipated as it impacts both autophagy-dependent and -independent endogenous viral antigen processing and presentation by MHC-II molecules.

T6BP silencing lowers the stability of newly formed MHC–peptide complexes but does not significantly influence MHC-II molecule cell-surface expression and internalization

Although T6BP silencing does not significantly alter the capacity of cells loaded with exogenous peptides to activate antigen-specific CD4⁺ T cells (Fig 1D and E right panels), we asked whether T6BP might influence the internalization of MHC-II molecules. Using flow cytometry, we first monitored on T6BP-silenced HeLa-CIITA cells, the expression levels of HLA-DR molecules using the L243 and TÛ36 antibodies that recognize mature HLA $\alpha\beta$ and immature HLA $\alpha\beta$ heterodimers associated with the invariant chain (Ii), respectively (Fig 2A, left panel: L243 and right panel: TÛ36). Using both antibodies, we noticed a slight increase in HLA-DR cell-surface expression levels on cells silenced for T6BP expression (Fig 2A). We next analyzed the effect of T6BP silencing on the internalization kinetics of MHC-II molecules. HeLa-CIITA cells treated with siCTRL or siT6BP were coated at 4°C for 30 min with the L243 antibody that has been shown to act as an agonist of MHC-II molecules leading to their cellular internalization (De Gassart *et al*, 2008). The cells were then incubated at 37°C to follow internalization of MHC-II molecules (Fig 2B) or maintained at 4°C to monitor the antibody drop-off (Fig 2C). The cells were collected at the indicated time points and stained at 4°C with a labeled secondary antibody to detect the remaining L243 antibody conjugated with MHC-II molecules at the cell surface (Fig 2B and C). At 4°C, the mean fluorescent intensity (MFI) of HLA-DR molecules remained stable (Fig 2C). By contrast, at 37°C, the MFI dropped reaching a plateau after 40 min in both experimental conditions (Fig 2B, left panel), thus suggesting that the L243 antibody induced the internalization of HLA-DR molecules in the presence or absence of T6BP expression. As previously, compared with control condition, the silencing of T6BP slightly increased the expression levels (MFI) of HLA-DR molecules on the cell surface. However, it did not influence the kinetics of internalization of HLA-DR (Fig 2B, right panel).

We then asked whether the silencing of T6BP might affect the stability of peptide-loaded HLA $\alpha\beta$ heterodimers. A fraction of peptide-loaded MHC-II $\alpha\beta$ heterodimers adopts a stable conformation resistant to dissociation by SDS at room temperature but not at 95°C (Germain & Hendrix, 1991). 48 h post-transfection, we thus analyzed the influence of siT6BP on the formation of SDS-stable HLA-DR $\alpha\beta$ heterodimers (Fig 2D). To this end, cells were pulsed with S³⁵ labeled methionine and cysteine, and then chased for 4 h, lysed and submitted to immunoprecipitation using TÛ36 that recognizes HLA $\alpha\beta$ heterodimers and HLA $\alpha\beta$ Ii complexes but not free α -, β -chains and Ii (Benaroch *et al*, 1995). Prior to loading onto the SDS–PAGE gel, samples were either boiled (B) or incubated at room temperature (not boiled, NB) for 30 min in SDS-sample buffer

(Fig 2D). Immediately after the pulse, boiling of the samples revealed the α , β and the fragment lip33/lip35 of the invariant chain (Fig 2D, B, chase 0 h). As expected from previous work, less α , β , and Ii were detectable after 4 h of chase (Fig 2D, NB, chase 4 h) (Benaroch *et al*, 1995). The nonboiled samples revealed the existence of SDS-resistant stable peptide-loaded HLA-DR $\alpha\beta$ heterodimers but only after 4 h of chase (Fig 2D, NB). Remarkably, in cells silenced for T6BP expression the band corresponding to SDS-resistant MHC $\alpha\beta$ heterodimers was greatly reduced as compared to cells transfected with siCTRL (Fig 2D, NB, chase 4 h), strongly suggesting that T6BP expression facilitates the formation of stable peptide-loaded HLA molecules. Overall, these results show that T6BP silencing does not influence MHC-II internalization and cellular expression levels, in a significant manner. However, it has a strong impact on the stability of peptide-loaded MHC-II $\alpha\beta$ heterodimers.

T6BP silencing dramatically alters the immunopeptidome of MHC-II molecules

Various parameters affect the quality of peptide-loaded MHC complexes, including the nature of the peptide itself (Roche & Furuta, 2015). We thus decided to analyze the global peptide repertoire (immunopeptidome) presented by MHC-II molecules. In addition, analyzing the immunopeptidome might also reveal whether T6BP silencing affects a broader range of potential antigens. To study the immunopeptidome, HeLa-CIITA cells were either mock-treated or transfected with CTRL or T6BP-silencing siRNA and MHC-II molecules were immunoprecipitated by using the TÛ39 antibody (specific to mature HLA-DP, DQ, and DR). Finally, the peptide ligands were identified using mass spectrometry (LC–MS/MS). To assess the intrinsic variability of the MHC-II ligandome in HeLa-CIITA cells, we analyzed simultaneously the ligandome of two samples from mock-treated HeLa-CIITA cells that were split 48 h prior to lysis and MHC-II immunoprecipitations (IP). In these settings, 57% of identified peptides were shared by both samples of mock-treated cells (Fig 3A, left panel). Two biological replicates of siRNA-treated cells were analyzed, one is presented in Fig 3. We observed that 1,349 peptides (representing 25% of the peptides) were presented by MHC-II molecules exclusively in HeLa-CIITA cells expressing T6BP (Fig 3A, right panel, siCTRL). Remarkably, in the absence of T6BP expression, 2,198 new MHC-II ligands (40% of the peptides) were identified (Fig 3A, right panel, siT6BP) and only 35% of the peptides (1914 peptides) were shared between control and the T6BP-silenced conditions (Fig 3A, right panel). Overall, siT6BP-treated cells shared significantly less MHC-II peptide ligands with the three other experimental conditions (Mock1, Mock2, or siCTRL) (Fig EV1A). Together these results show that, although there is an intrinsic variability of the MHC-II ligandome in cells, the absence of T6BP has a pronounced and dramatic influence on the repertoire of peptides presented by MHC-II molecules.

We then asked whether T6BP expression might affect the source of peptides, i.e., the set of proteins supplying peptides for MHC-II loading. To this end, we submitted the LC–MS/MS data to cell component enrichment analysis using Funrich software (Pathan *et al*, 2015). As expected from previous work (Dengjel *et al*, 2005; Marcu *et al*, 2021), according to Funrich annotation and as compared with the human proteome, in both siCTRL- and siT6BP-

treated cells, the MHC-II-ligand source proteins were enriched in cellular fractions belonging to membranes, secretory pathways (e.g., exosomes and vesicles) but also to the cytosolic compartment of the cell (Fig EV1B). In siCTRL-treated cells MHC-II source proteins were also augmented in nuclear fractions, which was not the case for siT6BP-transfected cells. By contrast, MHC-II-ligand source proteins

belonging to the cytoplasm were enriched in siT6BP-treated cells (Fig EV1B). Overall, this analysis shows that the bulk of MHC-II-ligand source proteins is provided by the same cellular fractions mainly membranes, secretory pathways, and the cytosol. However, the presence of T6BP might also favor the presentation of peptides derived from the nucleus.

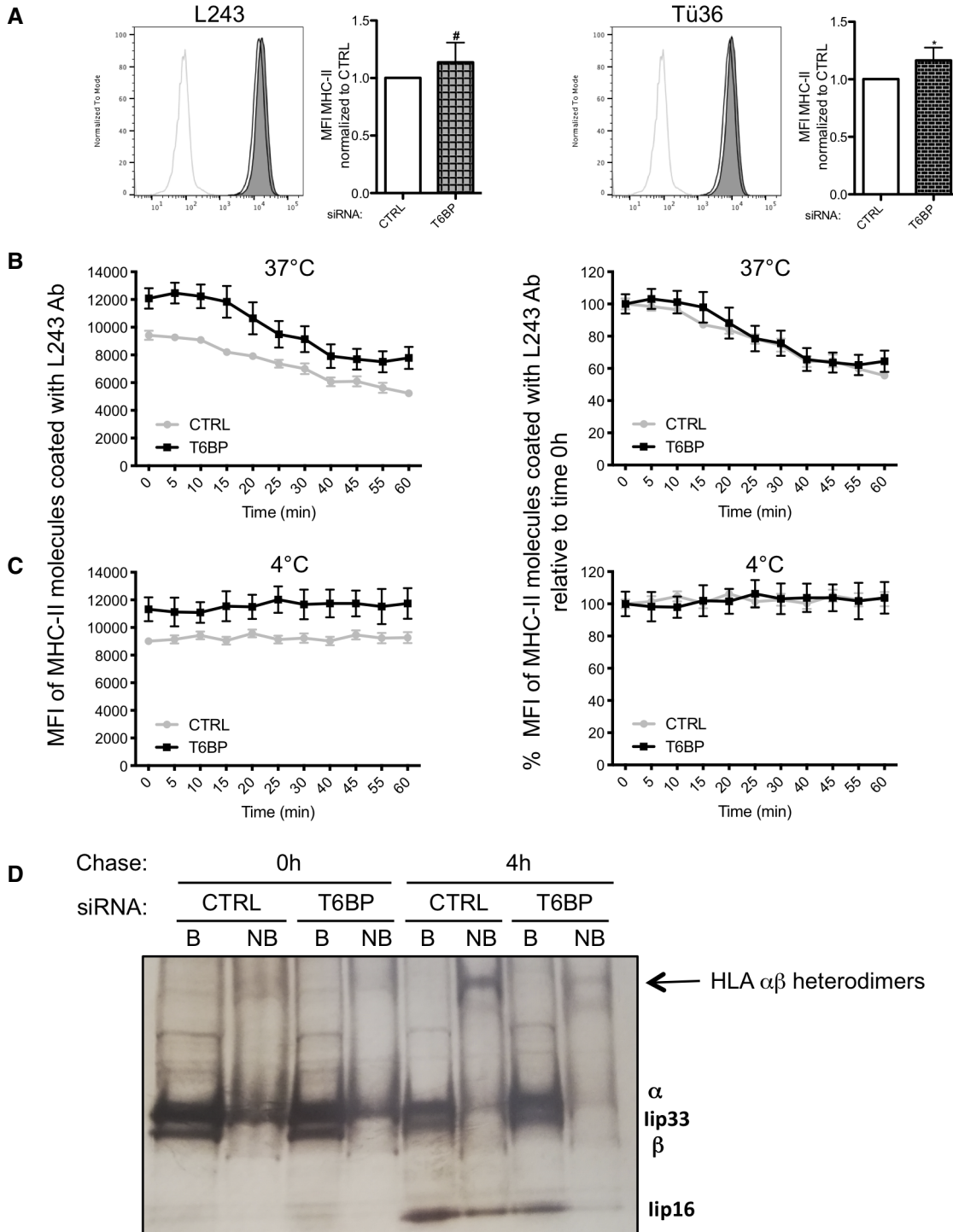


Figure 2.

Figure 2. T6BP silencing influences the stability of HLA $\alpha\beta$ dimers, mildly their cell-surface expression levels but has no impact on their internalization kinetics.

- A** Cell-surface expression of MHC-II molecules was assessed using flow cytometry. HeLa-CIITA cells were transfected with siCTRL and siT6BP. 48 h post-treatment, HLA-DR molecules were detected using L243 (left panels) and Tü36 antibodies (right panels) that recognize mature (HLA $\alpha\beta$ heterodimers) and both mature and immature (HLA $\alpha\beta$ and $\alpha\beta$ li complexes), respectively. Left, MFI of one representative experiment is presented as histogram. Light gray lines: isotype negative controls; black lines and filled gray lines: anti-MHC-II staining of siCTRL- and siT6BP-treated cells, respectively. Right, five biological replicates were combined and presented as the means (\pm SD) of mean fluorescent intensity (MFI) standardized to the control conditions. CTRL: control. Mann–Whitney's test; * $P < 0.05$; # $P > 0.05$.
- B, C** Internalization kinetics of cell-surface HLA-DR molecules. HeLa-CIITA cells were transfected as above. 48 h post-treatment, mature HLA-DR molecules were stained at 4°C using L243 antibody. Cells were then incubated at 37°C (B) or at 4°C (C). At indicated time points, cells were stained with a fluorescent secondary antibody at 4°C. Results are represented as MFI of MHC-II molecules stained with the L243 antibody remaining at the cell surface (B and C, left panels), or as percentage (%) of MFI relative to time 0 h (100%) (B and C, right panels). Results are presented (\pm SD) of technical replicates and representative of three independent experiments.
- D** T6BP silencing affects the formation of stable MHC-II-peptide complexes. HeLa-CIITA cells were transfected as above and pulse-labeled with ^{35}S -Met/Cys for 30 min, washed, and chased for 4 h at 37°C. MHC-II molecules were then immunoprecipitated using Tü36 antibody and analyzed on SDS–PAGE after incubation of the immunoprecipitated protein complexes with SDS at 95°C (B: boiled) or room temperature (NB: nonboiled) to visualize α , β , and li chains and SDS-resistant $\alpha\beta$ dimers, respectively. The bands corresponding to α , β , and li chains are indicated. The arrow indicates the SDS-resistant stable HLA $\alpha\beta$ heterodimers. This gel is representative of two independent experiments.

We then sought to analyze the influence of T6BP on the relative abundance and the quality, i.e., the affinity to MHC-II molecules, of peptides presented. However, peptides eluted from MHC-II molecules are variable in length and one core epitope required for MHC-II binding, usually 13 amino acid long, can be found in multiple peptides with N- and C-terminal extensions (Rammensee *et al*, 1999). To circumvent this limitation, we adapted a protocol, published by Alvaro-Benito *et al*, to identify the core epitopes within our datasets using the Peptide Landscape Antigenic Epitope Alignment Utility (PLATEAU) algorithm (Alvaro-Benito *et al*, 2018). A total of 864 and 1,245 unique core epitopes were identified in the groups Mock1/Mock2 and siCTRL/siT6BP, respectively. PLATEAU also allows calculating the relative abundance of the core epitopes based on the LC–MS/MS intensities of peptides containing the same core epitope. Between the two mock-treated samples, around 5% of the core epitopes showed a significant difference in their relative abundances (Fig 3B, left panel). Remarkably, between the siCTRL and siT6BP conditions, 55% of the core epitopes displayed a relative abundance that was significantly different between siCTRL and siT6BP conditions, with 436 and 246 epitopes more abundant in the siT6BP or siCTRL-treated cells, respectively, among 1,245 peptides (Fig 3B, right panel). Therefore, T6BP silencing influences both the peptide repertoire (Fig 3A) and the relative abundance of a majority of the core epitopes presented by MHC-II molecules (Fig 3B).

Having identified the core epitopes, using NetMHCIIpan4.0 algorithm (Reynisson *et al*, 2020), we next analyzed the relative binding affinities of exclusive peptides, identified in siCTRL and siT6BP conditions, to the HLA-DR β 1*0102 allele that is expressed by HeLa-CIITA cells. Strikingly, when T6BP is expressed (siCTRL), more than 90% of the epitopes were predicted to be HLA-DR β 1*0102 binders (26% and 65%, strong and weak binders, respectively). By contrast, in T6BP-silenced cells, below 50% of peptides were predicted to bind HLA-DR β 1*0102 (16% and 33%, strong and weak binders, respectively) (Fig 3C). Together, these results suggest that in the absence of T6BP, the peptides presented by HLA-DR β 1*0102 molecules have a predicted weaker relative affinity.

Note that we also analyzed on the same samples whether T6BP might influence the immunopeptidome of MHC-I molecules. Cells transfected with siCTRL or siT6BP and the two mock-treated samples were submitted to IP but using the pan anti-MHC-I antibody, W632, and the peptide ligands sequenced using LC–MS/MS. We did not observe a significant influence of T6BP on the percentage of shared or exclusive peptides comparing siCTRL/siT6BP conditions

(Fig EV2A). We further analyzed the relative affinities of the exclusive peptides bound to siCTRL- and siT6BP-treated cells. In contrast to MHC-II ligands, MHC-I molecules present short 9-mer peptides that correspond to the core epitope (Rammensee *et al*, 1999). We thus directly analyzed the relative affinities using the NetMHCpan 4.0 algorithm (Jurtz *et al*, 2017). The percentages of strong, weak, and nonbinder peptides were similar in control and T6BP-silenced cells (Fig EV2B). Therefore, the action of T6BP seems to be limited to the MHC-II-restricted antigen presentation pathway. T6BP expression has a strong influence on the peptide repertoire, the relative abundance, and the relative affinity of epitopes presented by MHC-II molecules.

T6BP silencing affects the cellular localization of the MHC-II

We then asked whether T6BP might play a role in the intracellular trafficking of MHC-II molecules before mature peptide-loaded MHC-II molecules reach the plasma membrane. To this end, using confocal microscopy analysis, we evaluated in HeLa-CIITA cells the effect of T6BP silencing on endo-lysosomal compartments. We first confirmed previous results (Petkova *et al*, 2017) showing that T6BP silencing leads to the accumulation of LC3-positive puncta corresponding to autophagosomes (Fig EV3A and B). Note that at a steady state in HeLa-CIITA-cells, T6BP did not co-localize with LC3⁺ puncta (Fig EV3B). We extended this observation using electron microscopy of the morphology of siRNA-treated cells and confirmed that large (around 1 μm in length) vesicles with a double membrane (with 20 to 30 nm interspace) accumulated in about 80% of the cells silenced for T6BP expression (Fig EV3E). These structures were not observed in the siCTRL-treated cells. Two independent experiments were performed and at least 40 cells for each treatment were analyzed. We then analyzed, by confocal microscopy, the sub-cellular localization of MHC-II molecules together with markers of autophagosomes, late endosomes and lysosomes. In HeLa-CIITA cells (Bania *et al*, 2003), MHC-II molecules, stained with an antibody to mature HLA-DR molecules (L243), localized in patches corresponding to intracellular vesicles that did not include T6BP (Fig 4A). Whatever the siRNA treatment, MHC-II molecules did not co-localize with LC3-positive puncta (Fig EV3C and D). However, when compared to the control condition, MHC-II molecules seemed to localize closer to the nucleus upon T6BP silencing (Fig 4A). We determined the average distance to the nucleus and the number of vesicles in more than 150 cells representing over 20,000 MHC⁺

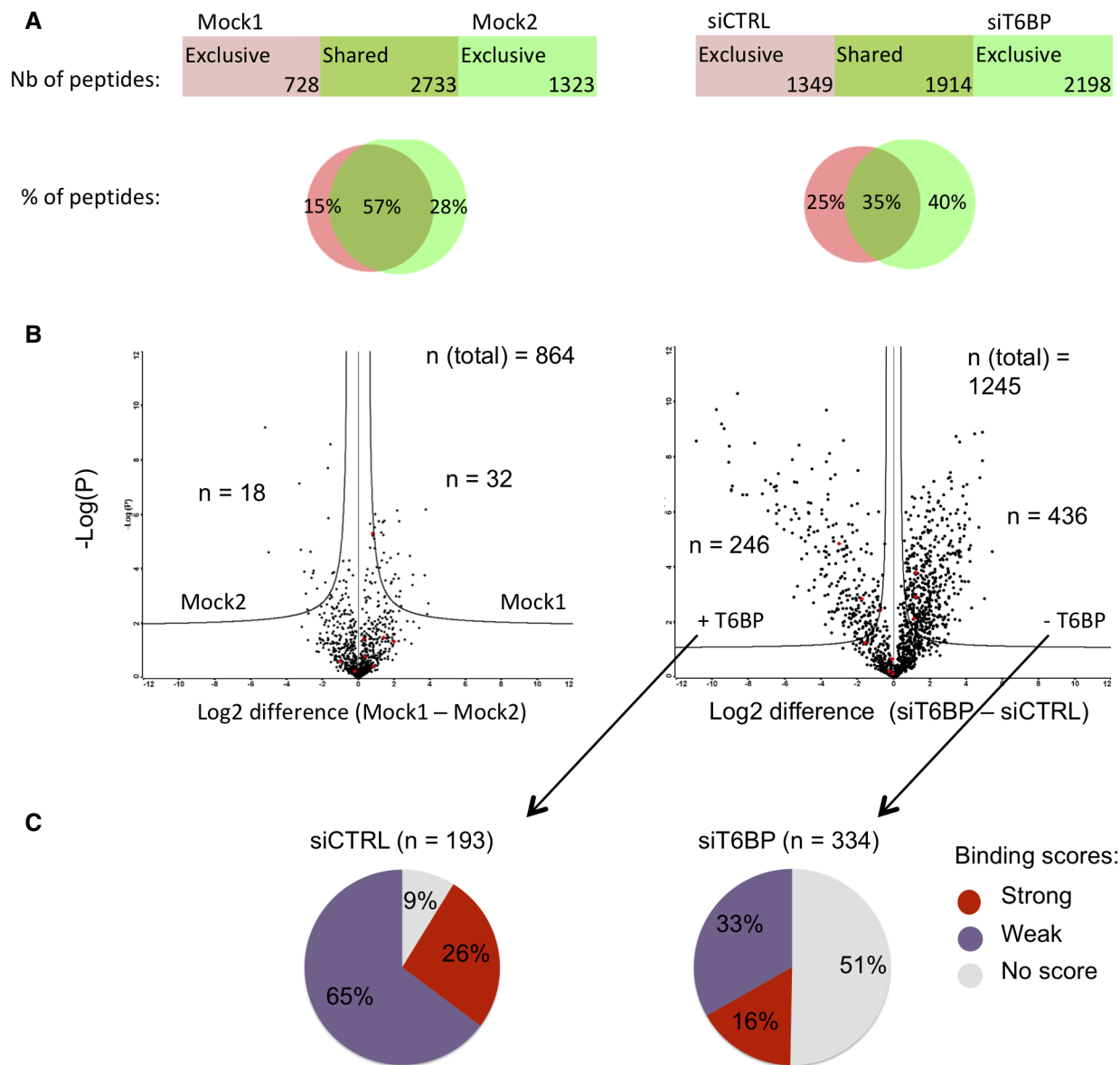


Figure 3. T6BP silencing alters the immunopeptidome of MHC-II molecules.

A Left panel, mock-treated HeLa-CIITA cells were split and cultured for 48 h (giving rise to Mock1 and Mock2), then cells were lysed, MHC-II molecules were immunoprecipitated using Tü39 antibody and the peptide ligands sequenced using mass spectrometry (LC-MS/MS). Right panel, HeLa-CIITA cells were transfected with siCTRL and siT6BP siRNA and were treated as in the left panel. The number and the percentage among sequenced peptides (Venn diagrams) of exclusive or shared peptides for each condition are presented.

B, C Quantitative (B) and qualitative (C) assessment of T6BP influence on the immunopeptidome. Data from (A) were submitted to PLAtEAU algorithm to allow identification and label-free quantification of shared consensus core epitopes. (B) Volcano plots showing the \log_2 fold change of core epitope intensity between siCTRL and siT6BP-treated cells (right panel) and Mock1 and Mock2 (left panel). For peptides exclusive to one or the other conditions, a background score was imputed to allow \log_2 fold-change presentation. An FDR of 0.01 and an SO of 0.2 as a correction factor for differences in the means were used. The resulting interval of confidence is highlighted by solid lines shown in each graph. The total number (n) of core epitopes and the number of epitopes with significant fold change are indicated. (C) Relative binding affinities, presented as pie charts, of exclusive core epitopes identified by PLAtEAU in siCTRL (left) and siT6BP (right) conditions (number of epitopes are indicated in brackets). NetMHCIIpan was used to predict the relative affinities to HLA-DRβ1*0102 expressed by HeLa-CIITA cells. The results are presented as stated from NetMHCIIpan analysis as strong (for strong binders), weak (for weak binders), and no score (for epitopes for which no binding score could be determined).

Data information: One representative experiment is shown out of two biological replicates. For each experiment, 5 technical replicates per sample were analyzed. Nb—number; %—percentage.

puncta (Fig 4B). We noticed a slight but significant decrease of MHC-II-positive vesicle distance to the nucleus upon T6BP silencing (Fig 4B). The numbers of MHC-II⁺ spots per cell were not

significantly different (Fig 4B). Using an anti-LAMP1 antibody, we then analyzed the effect of T6BP expression on late endo-lysosomal compartments. As compared to control cells, we observed a

significant relocalization of LAMP-1-positive vesicles at the proximity of the nucleus in T6BP-silenced cells (Fig 4C and D). The number of LAMP-1-positive vesicles was globally unchanged (Fig 4C and D).

We next asked whether the MIIC itself might be affected by T6BP silencing in HeLa-CIITA cells. The MIIC is a labile ill-defined acidified compartment that has been shown to be positive for multiple markers that do not always overlap (Roche & Furuta, 2015). We used LysoTracker that stains acidified compartments, CD63, a tetraspanin molecule anchored to the membrane of the intraluminal vesicles of the MIIC (Roche & Furuta, 2015), HLA-DM, the chaperone involved in MHC-II peptide loading, and MHC-II molecule staining to identify the MIIC. In the absence of T6BP, we observed a pronounced, statistically significant, relocalization of LysoTracker-positive vesicles close to the nuclei but the number of LysoTracker-positive vesicles was unchanged (Fig 4E and F). Remarkably, in siT6BP-treated cells, LysoTracker-positive vesicles showed increased co-localization with MHC-II molecules (Fig 4E and F). Upon T6BP silencing, CD63-positive vesicles were also strongly relocalized around the nucleus and showed an increased co-localization with MHC-II-positive puncta (Fig 4G and H). The number of CD63-positive vesicles was strongly reduced in T6BP-silenced cells (Fig 4H). Finally, we analyzed the influence of T6BP silencing on the cellular localization of HLA-DM. As for CD63, in T6BP-silenced cells, HLA-DM⁺ vesicles were strongly relocalized around the nucleus and their number was reduced as compared to mock-treated cells (Fig EV3F and G). In summary, in T6BP-silenced cells, LAMP-1⁺, HLA-DM⁺, CD63⁺, LysoTracker⁺ and MHC-II⁺ vesicles showed a repositioning at the proximity of the nucleus (Fig 4).

siT6BP silencing also induced a slight accumulation of EEA1⁺ early endosomes in the perinuclear region (Appendix Fig S2A and B). Whatever the treatment, no colocalisation between EEA1 and MHC-II was observed (Appendix Fig S2A and B). Also note that overall, T6BP-silencing did not significantly reduce the expression levels of the various markers analyzed using flow cytometry (Fig 2), WB (Fig 5), and IF (Appendix Fig S2C–H). Taken together these results show that T6BP expression influences the positioning of the MIIC, which is relocalized closer to the nucleus in the absence of T6BP. This repositioning of the MIIC could at least partially account for the defect of MHC-II maturation and could sustain the dramatic changes in the global MHC-II peptide repertoire, observed in the absence of T6BP.

T6BP silencing leads to exacerbated CD74 degradation in HeLa-CIITA cells

CD74 (Ii) is essential for the traffic and the maturation of MHC-II molecules within the cell (Bakke & Dobberstein, 1990; Lotteau et al, 1990; Neefjes et al, 1990; Roche et al, 1991). In the MIIC, CD74 degradation is also strictly regulated to ensure appropriate loading of MHC-II molecules with high-affinity peptides (Riese et al, 1996; Nakagawa et al, 1998; Shi et al, 2000; Manoury et al, 2003). We thus assessed the effect of T6BP silencing on CD74 expression. Note that in humans, among the four CD74 isoforms (Iip33, Iip35, Iip41, and Iip43) Iip33 is the most abundant (Thibodeau et al, 2019). As previously, HeLa-CIITA cells were transfected with siRNAs, and CD74 expression was assessed by WB. In control cells, Iip33 was readily detected together with its cleavage

product Iip16 (Fig 5A). By contrast, upon T6BP silencing, Iip33 and Iip16 detection was strongly decreased (Fig 5A). Normalized to the housekeeping gene (actin), the decrease in Iip33 expression reached up to 50% (Fig 5A, right panel). As a control, using WB, we also assessed the expression level of HLA-DR molecules. As expected from our flow cytometry and microscopy results (Figs 2 and 4, respectively), the global expression of HLA-DR molecules was similar in siCTRL- and siT6BP-treated cells (Fig 5B). In addition, we asked whether T6BP silencing might also affect the expression of HLA-DM, the chaperone involved in quality control of peptide loading on MHC-II molecules. As for HLA-DR, the expression levels of HLA-DM were not affected by the extinction of T6BP expression (Fig 5C). Using confocal microscopy, we confirmed that T6BP-silenced cells exhibit about 50% lower expression levels of CD74 than control cells (Fig EV4A and B). Note that, in control cells, the T6BP staining did not co-localize with CD74 (Fig EV4A and C).

We then asked at which level CD74 expression was affected, i.e., at the RNA or protein levels. To this end, we first used RT-qPCR to monitor CD74 and T6BP mRNA relative quantities in control and T6BP-silenced HeLa-CIITA cells. As anticipated T6BP mRNA levels were strongly reduced in siT6BP-treated cells (Fig EV4D). By contrast, mRNA levels of CD74 were not influenced by T6BP silencing (Fig EV4E). We next analyzed whether CD74 expression could be reversed, in siT6BP-silenced cells, upon treatment with drugs inhibiting lysosomal or proteasomal degradation, using chloroquine or epoxomicin, respectively. As expected, since the proteolytic cleavages of CD74, required for MHC-II peptide loading are dependent on cathepsin activities (Riese et al, 1996; Nakagawa et al, 1998; Shi et al, 2000; Manoury et al, 2003), the treatment of control cells with chloroquine allowed the detection of the intermediate degradation fragment Iip22 (Fig 5D). Remarkably, when compared to control untreated cells, chloroquine treatment allowed a strong recovery of both Iip33 and Iip16 expression in siT6BP-treated cells (Fig 5D). By contrast, although proteasomal inhibition induced, as expected, the accumulation of polyubiquitinated proteins (Appendix Fig S3), epoxomicin treatment did not affect the expression levels of CD74 (Fig 5D).

These results prompted us to analyze the kinetics of degradation of CD74 complexes. To address CD74 proteolysis in control and T6BP silenced HeLa-CIITA cells, 48 h post-transfection cells were pulsed with S35 Met/Cys for 30 min and chased for different times. HLA-CD74 complexes were isolated by immunoprecipitation with TÛ36 antibody and in a second set of experiments CD74 was first immunoprecipitated, together with HLA molecules, using TÛ36 antibody and then reimmunoprecipitated using VICY1 antibody, which binds the cytosolic tail of CD74. As shown in Fig 5E, in control cells, CD74 isoforms (Iip41 and Iip33) and their fragments (Iip16) appeared in the pulse and during the chase. By contrast, when HeLa-CIITA was silenced for T6BP much less Iip41, Iip33 and Iip16 were detected. In fact, in the control conditions, the invariant chain degradation product, Iip16, was detected mostly after 1 h of chase (Fig 5E). By contrast, Iip16 was immediately detected after the pulse (time 0 h) in the T6BP-silenced cells (Fig 5E) suggesting a rapid CD74 degradation (see quantification on the right panel). Furthermore, when HLA/CD74 complexes were first immunoprecipitated with TÛ36 antibody and reimmunoprecipitated with VICY1 antibody, much less CD74 (Iip33) was detected in T6BP silenced cells (Fig 5F). Altogether these results suggest a much faster degradation

of CD74, either free or associated with MHC-II molecules, in the absence of T6BP.

Interestingly, the expression of CD74 has been shown to influence both the cellular trafficking and the immunopeptidome of MHC-II molecules (Muntasell *et al*, 2004). It has also been suggested that in cells lacking MHC-II expression, CD74 might regulate endosomal maturation (Schröder, 2016).

T6BP interactome reveals novel binding partners

To decipher the mechanism by which T6BP influences MHC-II-restricted endogenous antigen presentation, we decided to define the interactome of T6BP in HeLa-CIITA cells. To this end, HeLa-CIITA cells were transfected with a plasmid encoding GFP-T6BP, a construct that was previously functionally characterized

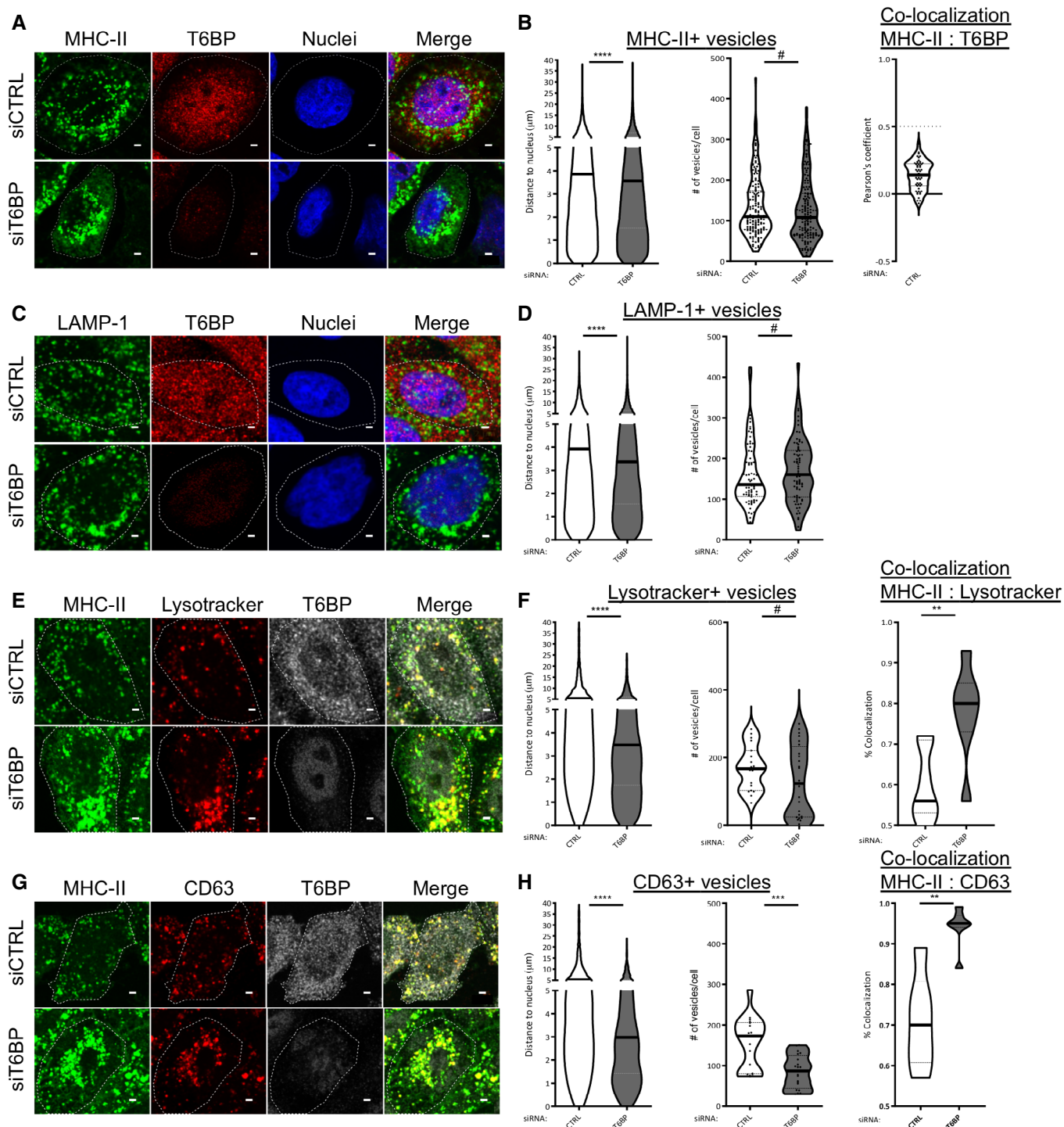


Figure 4.

Figure 4. T6BP silencing leads to perinuclear relocalization of the MHC-II.

- A MHC-II and T6BP expressions were assessed using confocal microscopy. HeLa-CIITA cells were transfected with control and T6BP-silencing siRNAs. 48 h post-treatment, MHC-II and T6BP were detected using L243 and anti-T6BP antibodies, respectively, and revealed with species-specific secondary antibodies. Nuclei were stained using DAPI.
- B Quantitative analysis using in-house ImageJ script displaying distance of each MHC-II⁺ vesicles to the nucleus and number of vesicles per cell. At least 20,000 vesicles from 160 cells corresponding to five biological replicates were analyzed. Right panel, quantification in the siCTRL cells of the co-localization between MHC-II⁺ and T6BP⁺ dots using Pearson's coefficient where the dotted lines (at 0.5) indicate the limit under which no significant co-localization is measured (number of cells = 54).
- C As in A, T6BP and LAMP-1 expressions were analyzed.
- D The localization of LAMP-1⁺ vesicles and the number of vesicles per cell were quantified as in B. At least 2000 vesicles from 20 cells corresponding to two biological replicates were analyzed.
- E As in A, adding LysoTracker staining.
- F As in B, quantitative analysis of LysoTracker⁺ vesicles: localization to the nucleus and number of vesicles per cell. Co-localization of LysoTracker⁺ vesicles with MHC-II⁺ puncta was analyzed using JACoP plugin (scales start at 0.5 above which the % of co-localization is considered significant); a number of vesicles >2000 from at least three biological replicates were analyzed corresponding to 20 cells.
- G As in E, CD63 and MHC-II expressions were assessed.
- H Quantitative analysis as represented in F. At least 2000 vesicles from 20 cells corresponding to two biological replicates were analyzed.

Data information: In graphs representing the number of vesicles per cell, each dot displayed corresponds to a single cell. Within the violin plots, continuous and dotted lines correspond to medians and quartiles, respectively. Scale bars: 2 μ m. CTRL—control. Mann–Whitney's test; * $P < 0.05$; ** $P < 0.002$; *** $P < 0.0003$; **** $P < 0.0001$; # $P > 0.05$.

(Morriswood *et al*, 2007), and as negative control the same plasmid encoding GFP (Appendix Fig S4A). We then performed a large-scale immunoprecipitation (IP) using GFP as a tag. Three biological replicates were performed. As a quality control, the lysates and the various fractions of the immunoprecipitation procedure were analyzed using Coomassie blue staining and anti-GFP staining in WB (Appendix Fig S4B). The immunoprecipitation products of the three replicates (presented in Appendix Fig S4C) were then submitted to mass spectrometry (LC–MS/MS) analysis to identify the proteins interacting with GFP-T6BP. The Uniprot *Homo sapiens* database was used to assign a protein name to the peptides sequenced by MS. The results were compared against the 3 IP replicates of GFP-transfected cells and a bank of 8 control experiments, also performed with GFP-Trap agarose magnetic beads, using the online contaminants database CRAPome.org (Mellacheruvu *et al*, 2013). Using a fold-change (FC) threshold of ≥ 10 and a Significance Analysis of INTeractome (SAINT) probability threshold of ≥ 0.8 (Choi *et al*, 2011), we identified 116 high-confidence T6BP proximal proteins (Fig 6 and Dataset EV1). These included previously known T6BP-interactants such as the E3 ligase ITCH (Shembade *et al*, 2008), the kinase TBK1 (Richter *et al*, 2016), and TRAF2, all involved in NF- κ B signaling pathways (Shembade *et al*, 2010). This screen also confirmed that T6BP interacts with the autophagy receptor p62 (SQSTM1) (Mildnerberger *et al*, 2017). It revealed novel potential partners that might bind directly or as part of larger T6BP-associated protein complexes. These candidates could be grouped in 6 major functional cellular pathways based on Ingenuity (Fig 6). As expected, from the known T6BP functions, some candidate partners were enriched in the ubiquitin/proteasome (P -value = 3,16E-18) and NF- κ B signaling (P -value = 1,15E-02) pathways but also in the unfolded protein response (UPR)/protein folding (P -value = 2,69E-04), endocytosis (P -value = 6,03E-05), and antigen presentation (P -value = 2,34E-06) pathways (Fig 6). The antigen presentation group includes HLA-A, -C, -DQ α 1, -DR β 1 molecules (Fig 6). In the UPR/protein folding group, the ER-resident chaperone protein Calnexin (CANX) is 22 times enriched in T6BP-GFP IP as compared to GFP only IP (Fig 6 and Appendix Table S1). CANX drew our attention because: (i) it has been shown to interact with CD74 (Anderson & Cresswell, 1994) and (ii) the inhibition of CANX/CD74 interaction

induces CD74 degradation without influencing the formation of MHC-II complexes (Romagnoli & Germain, 1995).

T6BP and Calnexin interaction is observed in professional APC and relies on Calnexin cytosolic tail expression

To verify that CANX interacts with T6BP, as previously, we immunoprecipitated GFP-T6BP and GFP from HeLa-CIITA transfected cells and analyzed, using WB, the presence of Calnexin in the immunoprecipitated fractions. The IP of the GFP-transfected cells leads to the immunoprecipitation of a larger GFP-positive fraction than the IP of the T6BP-GFP-transfected cells (Appendix Fig S4D, anti-GFP Ab). Nonetheless, we observed a 3-fold enrichment of CANX in cells transfected with GFP-T6BP as compared to GFP-transfected cells (Appendix Fig S4D). In HeLa-CIITA cells, we further confirmed the specific interaction between T6BP and CANX using two different techniques: (i) by immunoprecipitation of endogenous T6BP and endogenous CANX, we revealed that the IP fractions of anti-T6BP and anti-CANX IPs contained CANX and T6BP, respectively (Fig 7A and B); (ii) by proximity ligation assay (PLA) on control cells and siT6BP-transfected cells a specific T6BP/CANX interaction was detected only in cells expressing T6BP (Fig 7C). To demonstrate that T6BP/CANX interaction is not restricted to HeLa-CIITA cells, we then immunoprecipitated endogenous T6BP and CANX from two professional APCs, namely B cells and DC. As in HeLa-CIITA, we revealed in the anti-T6BP and anti-CANX IP fractions, of both B cells and DC, the presence of CANX and T6BP, respectively (Fig 7A and B). Altogether, these results strongly support that CANX interacts with T6BP directly or as part of a larger protein complex.

In order to characterize the molecular interactions between CANX and T6BP, we then engineered a construct containing solely the transmembrane domain and the cytosolic tail of CANX fused to a GST tag. Since T6BP expression is mainly cytosolic, we reasoned that T6BP and CANX might interact through the cytosolic tail of CANX. The GST-TM-cytosolic Tail construct was transfected in HeLa-CIITA cells and immunoprecipitated using anti-GST antibodies. Western blotting revealed that T6BP is co-immunoprecipitated with anti-GST in cells transfected with GST-TM-cytoTail-CANX and not in cells transfected with the control vector (Fig 7D). Taken together, we demonstrate here that T6BP interacts with CANX through its

cytosolic tail. We propose that, through the binding to the cytosolic tail of CANX, T6BP promotes the interaction of CANX with CD74 leading to CD74 stabilization.

Calnexin silencing induces CD74 degradation and reduces MHC-II-restricted antigen presentation to CD4⁺ T cells

Finally, we investigated the direct role of CANX in MHC-II-restricted antigen presentation. To this end, we screened several siRNA targeting

Calnexin and identified an siRNA whose transfection led to a strong decrease in CANX expression (siCANX) (Appendix Fig S4E). Using WB, we first analyzed the influence of CANX-silencing on CD74 expression. In siCANX-treated cells, we observed a strong reduction in CD74 expression levels (Fig 7E) reminiscent of what we observed in cells silenced for T6BP expression (Figs 5A and D, and 7E). Note that neither siT6BP nor siCANX transfections lead to an increased expression of CANX or T6BP, respectively (Fig 7E and Appendix Fig S4E). To monitor the influence of Calnexin on antigen presentation, HeLa-

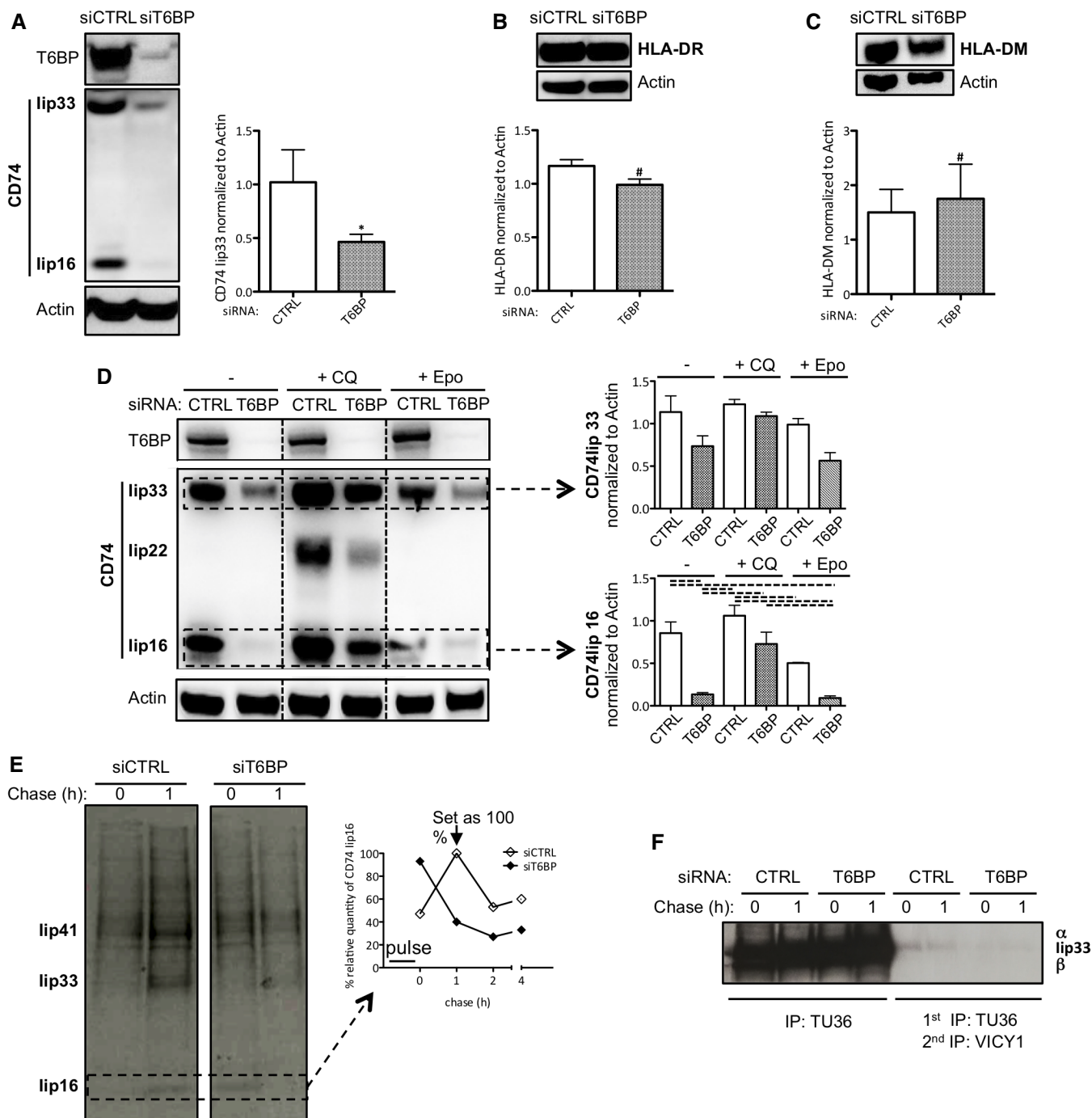


Figure 5.

Figure 5. T6BP silencing leads to exacerbated CD74 (II) degradation.

- A CD74 expression was assessed using Western Blot. HeLa-CIITA cells were transfected with siCTRL and siT6BP. 48 h post-treatment, the lip33 CD74 isoform, a degradation product (lip16), T6BP, and actin were detected using indicated antibodies. Left panel, a representative Western Blot experiment is shown. Right panel, expression levels of five biological replicates were quantified using ImageJ and are presented as mean ratios (\pm SD) of CD74 to actin used as control housekeeping gene expression.
- B As in (A) assessing HLA-DR and actin expression levels. Top panel, a representative Western Blot experiment is shown. Bottom panel, in three biological replicates, HLA-DR expression was quantified using ImageJ and is presented as mean ratios to actin (\pm SD).
- C As in (B) assessing HLA-DM and actin expression levels. Bottom panel, HLA-DM expression was quantified in three biological replicates and presented as mean ratios to actin (\pm SD).
- D CD74 expression is partially recovered by blocking lysosomal acidification. As in (A), following siRNA transfection of HeLa-CIITA cells, CD74 expression was assessed. The last 16 h prior to harvesting, cells were treated with chloroquine (CQ) or epoxomicin (Epo). Left panel a representative experiment is shown, membranes were blotted using anti-T6BP, -CD74, and -actin antibodies. The different degradation fragments of CD74 are indicated (lip33, lip22, and lip16). Right panel, expression levels of lip33 (top) and lip16 (bottom) were quantified in three biological replicates using ImageJ and are presented as mean ratios of each fragment to actin (\pm SD).
- E, F Analysis of CD74 proteolysis. HeLa-CIITA cells were transfected with siCTRL and siT6BP. 48 h post-treatment, cells were pulsed for 30 min with ^{35}S -Met/Cys, washed, and chased for 1, 2, and 4 h. HLA-DR/CD74 complexes were first immunoprecipitated using T \dot{u} 36 antibody (E) and then reimmunoprecipitated with VICY1 antibody (F). Samples were boiled and analyzed using SDS-PAGE. The bands corresponding to CD74 isoforms (lip41 and lip33) and the cleavage products (lip16) are indicated. (E right panel) lip16 expression was quantified using ImageJ and presented as a percentage of lip16 normalized to the highest quantity of lip16 detected after 1 h of chase in the control condition. Results are representative of two biological replicates. li: invariant chain (CD74); CTRL: control.

Data information: (A-C) Wilcoxon's test; * $P < 0.05$; # $P > 0.05$. (D) One-way ANOVA statistical test combined with the Bonferroni's multiple comparison test was applied. Dotted lines indicate statistically significant differences between conditions. Source data are available online for this figure.

CIITA cells were transfected with siCANX side by side with siCTRL or siT6BP used as negative and positive controls, respectively. As in Fig 1E, the cells were then transfected with the plasmid encoding the HCMV pp65 antigen and co-cultured with the anti-pp65 CD4⁺ T cell line. CANX-silencing induced a marked inhibition of CD4⁺ T cell activation by pp65-transfected cells (Fig 7F, left and middle panels). By contrast, the inhibition of CANX expression did not influence the capacity of peptide-loaded cells to activate pp65-specific CD4⁺ T cells (Fig 7F right panel), confirming that CANX inhibition influences neither HLA-DR expression nor the viability of the cells. We show here that T6BP silencing affects CANX functions resulting in CD74 degradation and aberrant MHC-II peptide loading and antigen presentation to CD4⁺ T cells.

Discussion

We demonstrate here that T6BP regulates the loading and presentation of endogenous viral antigens by MHC-II molecules. This function of T6BP in antigen presentation has a direct implication in the activation of virus-specific CD4⁺ T cells. The action of T6BP is broader than what we initially anticipated as it affects the presentation of various antigens whose processing is dependent or independent on autophagy degradation. We further show that T6BP shapes the immunopeptidome of MHC-II molecules. We provide evidence that T6BP controls MHC-II molecule peptide loading in particular through its interaction with the cytosolic tail of CANX that stabilizes the invariant chain. However, this is probably not the only way by which T6BP affects MHC-II-restricted antigen presentation as it also participates in the regulation of the trafficking of MHC-II-loading compartments and more globally of acidified vesicular compartments.

We previously reported that HIV-infected cells present MHC-II-restricted HIV Gag- or Env-derived antigens to HIV-specific CD4⁺ T cells (Coulon *et al*, 2016). The processing of these native antigens does not rely on the autophagy pathway. However, when targeted

to autophagosomes, using LC3, HIV Gag processing is dependent on autophagosomal degradation. In fact, using DC and HeLa-CIITA cells we showed that as compared to native HIV Gag protein, the targeting of HIV Gag to autophagosomes leads to more robust activation of Gag-specific T cells (Coulon *et al*, 2016). We concluded that depending on the cellular localisation, the same antigens may be degraded by various endogenous routes leading to MHC-II loading. We reveal here that T6BP modulates Gag antigen presentation independently of its cytosolic or autophagosomal cellular localisation. Likewise, T6BP affects the presentation of a HCMV pp65-derived peptide. Our analysis of the immunopeptidome of HeLa-CIITA cells uncovers that T6BP has a broad influence on the repertoire and relative abundance of the peptides presented by MHC-II molecules. Without excluding the possibility, these observations do not indicate whether T6BP also affects the exogenous pathway of antigen presentation by MHC-II molecules. Indeed, others and we (Fig EV1) have demonstrated that the landscape of peptides naturally presented by MHC-II molecules contains a large fraction of peptides derived from intracellular proteins (Rudensky *et al*, 1991; Rammensee *et al*, 1999; Muntasell *et al*, 2002). In our model system, HeLa-CIITA cells, we could not ask whether the silencing of T6BP affects the exogenous pathway because these cells lack the ability to present exogenous viral antigens to CD4⁺ T cells (Coulon *et al*, 2016). This is a weakness but also a strength of this model system since it allowed focusing our work on the endogenous pathway. Nevertheless, we intended to ask whether T6BP might affect antigen presentation by primary APCs. We used several means to silence T6BP in MDDCs including siRNA and shRNA. Unfortunately, whatever the protocol and independently of T6BP expression, the tools used to transfect or to transduce MDDC induced maturation of the cells and affected the traffic of MHC-II molecules, which prohibited drawing any conclusion on the potential role of T6BP in MDDCs. Nonetheless, our results strongly suggest that at least in epithelial cells that can turn into APCs upon inflammation (Wijdeven *et al*, 2018), T6BP expression shapes the peptide repertoire, the relative abundance, and the relative affinity of epitopes presented

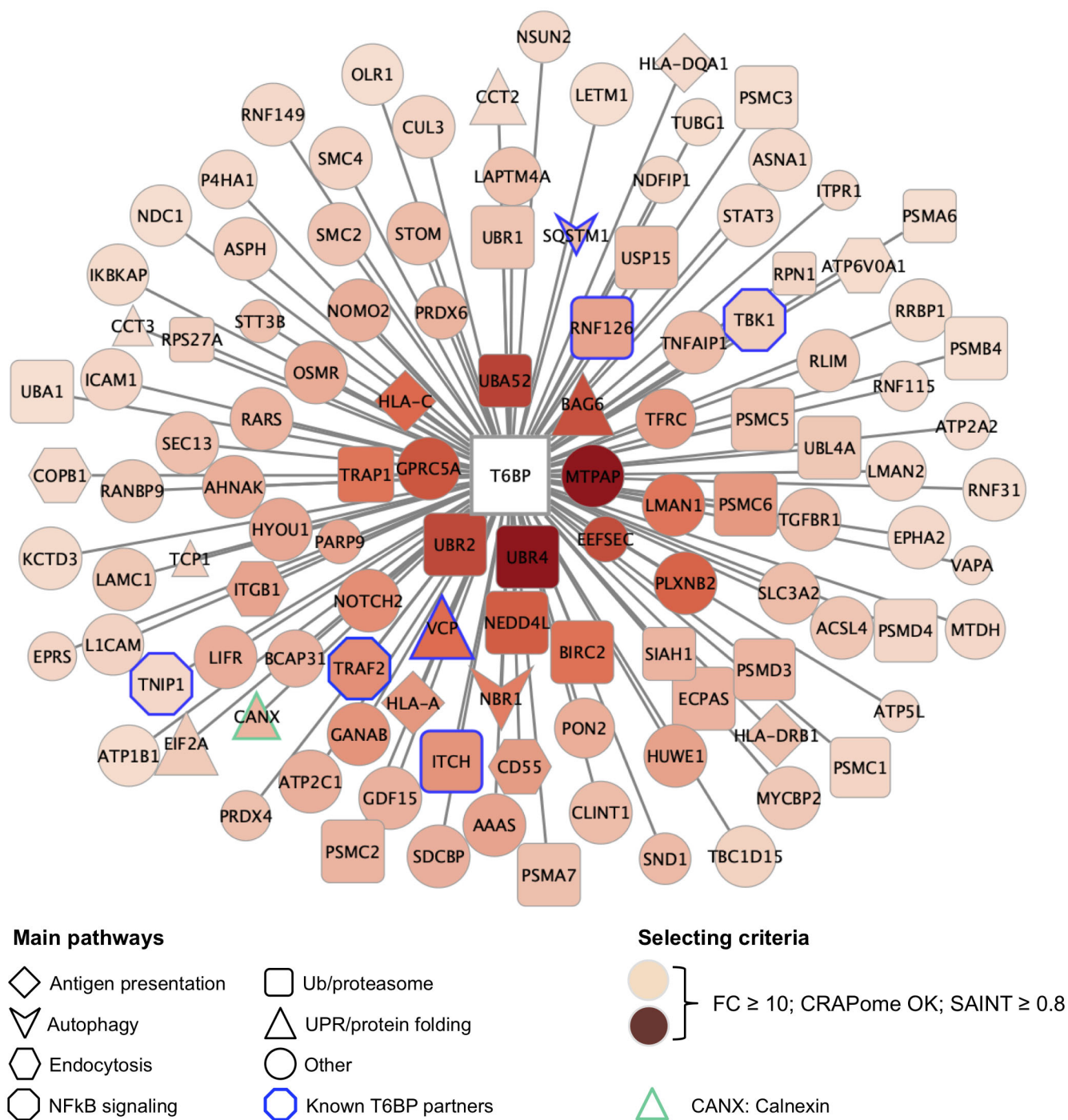


Figure 6. T6BP interactome reveals novel binding partners.

Diagram of the T6BP protein interaction network identified by immunoprecipitation followed by LC-MS/MS and represented using Cytoscape. T6BP (white) coupled to GFP was immunoprecipitated using anti-GFP camel antibodies (GFP-Trap Chromotek). GFP alone was used as control. Proteins were considered as relevant partners based on the following criteria: at least 2 peptides were identified by LC-MS/MS, the fold change (FC) to the GFP control condition ≥ 10 , SAINT probability threshold ≥ 0.8 . For data analysis, the Resource for Evaluation of Protein Interaction Networks (REPRINT) and its contaminant repository (CRAPome V2.0) were used. The edge's length is inversely proportional to the FC score (short edge = high FC) and the node's color intensity is directly proportional to the FC score (the more intense the higher the FC). The size of the node is directly proportional to the SAINT score (lower confidence = smaller node). Blue border indicates previously described partners of T6BP. The shape of the node highlights the functional pathway in which the candidate protein is enriched based on Ingenuity. Green border indicates Calnexin = CANX.

by MHC-II molecules. Indeed, our immunopeptidomic data suggest that the expression of T6BP favors the loading of peptides with a higher binding capacity to HLA-II molecules. As expected, based on

previous work with cell lines (Alvaro-Benito *et al*, 2018) or analyzing tissue samples (Marcu *et al*, 2021), we observed a natural variation of the MHC-II immunopeptidome between two mock-treated

samples with about 60% of shared peptides. However, in these mock samples, we did not notice a significant difference in terms of the relative quantity of core epitopes. This is in sharp contrast to the comparison of wild-type and T6BP-silenced cells where half of the MHC-II binding core epitopes were differentially presented. Remarkably, we also observed a natural variation of the immunopeptidome of MHC-I molecules, with about 50% of shared peptides. Notably, T6BP silencing did not have a strong influence on the repertoire of peptides presented by MHC-I molecules, as the percentage of shared

peptides with the control siRNA-treated cells was also around 50%. In addition, the affinity of MHC-I ligands was comparable in wild-type cells and cells silenced for T6BP expression. Our results strongly suggest that the action of T6BP is restricted to the MHC-II antigen presentation pathway and affects both the abundance and the affinity of core epitopes to HLA molecules.

The chaperones HLA-DM and the invariant chain (Ii) CD74 tightly regulate the loading of peptides on MHC-II molecules. Previous studies have shown that the levels of expression of both HLA-

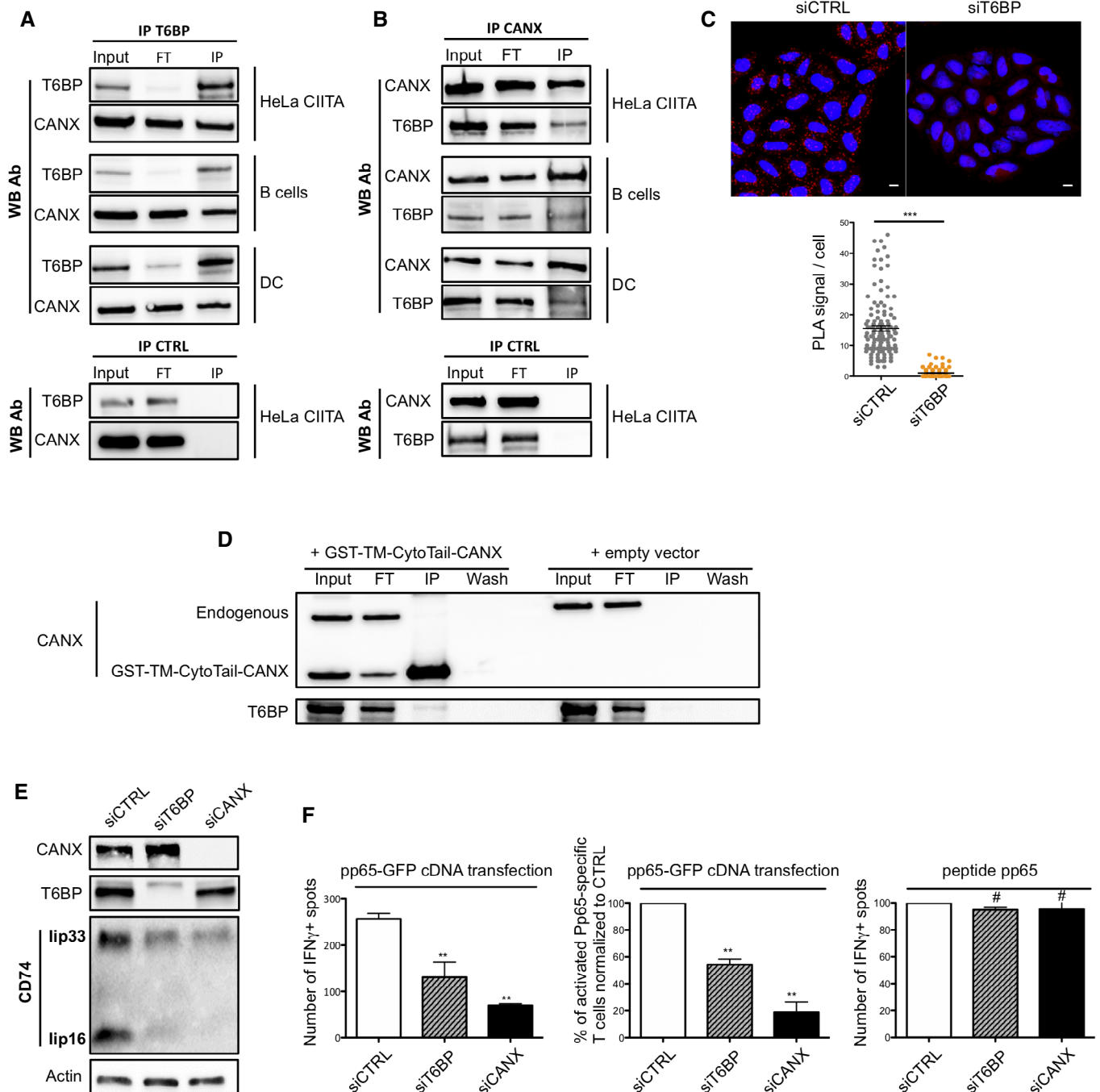


Figure 7.

Figure 7. Calnexin (CANX) interacts with T6BP through its cytosolic tail and stabilizes CD74 thus favoring MHC-II-restricted antigen presentation to CD4⁺ T cells.

- A, B CANX co-immunoprecipitates with T6BP in model and professional APCs. Endogenous T6BP was immunoprecipitated from HeLa-CIITA, B (DG-75), and dendritic-like (KG-1, DC) cells. The input, the flow-through (FT), and the immunoprecipitation (IP) fractions were analyzed by Western blot using the indicated antibodies. Bottom panels, control IPs using the beads without antibody (IP CTRL) are presented for each IP. (B) As in (A) but using anti-CANX Ab for the IP. For A and B, one representative experiment out of three biological replicates is shown.
- C CANX interacts with T6BP using proximity ligation assay (PLA). 48 h post-transfection with the indicated siRNAs, HeLa-CIITA cells were fixed, stained with anti-T6BP and anti-CANX antibodies and proximity revealed using PLA (Duolink). Nuclei were stained using DAPI. Top panel, two representative fields are shown. Bottom panel, quantitative analysis using ImageJ displaying the number of PLA per cell. The continuous line indicates the mean (\pm SEM). PLA was quantified in at least 130 cells corresponding to three biological replicates. Scale bars: 10 μ m. CTRL: control; Mann–Whitney's test; *** P < 0.0003.
- D Calnexin interacts with T6BP through its cytosolic tail. HeLa-CIITA cells were transfected with a plasmid encoding the GST-tagged transmembrane (TM) and cytosolic (CytoTail) domains of CANX (GST-TM-CytoTail-CANX) or the vector not encoding TM-CytoTail-CANX as control and immunoprecipitated with anti-GST antibodies. The input, FT, the wash, and the IP fractions were analyzed by Western blot and revealed using the indicated antibodies. One representative experiment out of three biological replicates is shown.
- E Silencing of T6BP does not influence CANX expression levels while silencing of CANX reduces the level of CD74 expression. HeLa-CIITA cells transfected with the indicated siRNAs and samples analyzed, 48 h post-transfection, by Western blot with the indicated antibodies. These western blot results are representative of at least three biological replicates.
- F CANX-silencing dampens MHC-II-restricted antigen presentation to CD4⁺ T cells. HeLa-CIITA cells were treated with the indicated siRNAs and transfected with a plasmid encoding pp65 HCMV antigen fused to GFP. HeLa-CIITA cells were then co-cultured with pp65-specific T cells. Left panel, a representative experiment is shown. The mean of three technical replicates (\pm SD) is shown. Middle, three biological replicates are combined and presented as the mean percentage (\pm SD) of activated cells producing IFN γ normalized to CTRL conditions. Right panel, influence of T6BP silencing on peptide presentation by HeLa-CIITA cells. The cognate peptide was added exogenously (pp65, 0.5 μ g/mL) on siRNA-treated cells (2 h, 37°C), washed and T cell activation monitored using IFN γ -ELISPOT. Three biological replicates are combined and presented as the mean percentage (\pm SD) of activated cells producing IFN γ normalized to CTRL conditions. Data information: The background secretions of IFN γ by CD4⁺ T cells co-cultured with mock-treated HeLa-CIITA cells were used as negative controls and subtracted. CTRL—control. Wilcoxon's test; ** P < 0.01; # P > 0.05.

Source data are available online for this figure.

DM and CD74 affect the repertoire and the affinity of the peptides presented by various HLA-DR and HLA-DQ alleles (Ramachandra *et al*, 1996; Muntasell *et al*, 2004; Alvaro-Benito *et al*, 2018). Remarkably, in the absence of T6BP, we noticed a reduced expression level of CD74 whereas HLA-DM and HLA-DR expression levels remained unchanged. Overall, we did not observe a significant influence of T6BP silencing on the expression levels of other intracellular markers/proteins than CD74. Our analysis of the expression kinetics of MHC-II complexes, using pulse/chase experiments, further showed that the lack of T6BP induces a rapid and exacerbated degradation of CD74. The expression levels of CD74 could be rescued by inhibiting lysosomal acidification but not proteasomal functions suggesting that CD74 is aberrantly degraded in endolysosomes in T6BP-depleted cells. These observations probably explain the modifications of the immunopeptidome and the instability of peptide-loaded MHC-II $\alpha\beta$ heterodimers, observed in the absence of T6BP expression. However, the diversity of the immunopeptidome could also be due to variations in the origin of the peptides presented by MHC-II molecules (Muntasell *et al*, 2004), in particular, since we observed a global modification of the cellular distribution of acidified vesicular compartments in the absence of T6BP. Although we observed, using functional enrichment analysis (Funrich, Fig EV1), a slight influence of T6BP silencing on the cellular distribution of the source protein of MHC-II ligands, this cannot by itself explain the effects of T6BP on the peptide repertoire. In particular since, T6BP expression also dictates the relative affinity of peptides presented by MHC-II molecules. Overall, our observations suggest that T6BP expression influences the degradation kinetics of CD74 with a direct influence on the diversity and affinity of the immunopeptidome of MHC-II molecules.

The ER chaperone CANX that participates in the quality control of protein folding in the ER has been shown to play an important role in the assembly of the nonameric MHC $\alpha\beta$ -CD74 complexes (Arunachalam & Cresswell, 1995). CANX retains and stabilizes

CD74 in the ER until it assembles with the MHC α - and β -chains (Romagnoli & Germain, 1995). It also binds newly synthesized α - and β -chains of HLA molecules until it forms, with CD74, a complete nonamer (Anderson & Cresswell, 1994). Interestingly, it has been shown that the treatment with Tunicamycin or the expression of CD74 mutants, lacking N-linked glycosylation, both impeding the interactions with CANX, can induce CD74 degradation (Romagnoli & Germain, 1995). We corroborate here that CANX influences CD74 expression. Using siRNA silencing, we provide a direct demonstration that the lack of CANX expression induces CD74 degradation. Furthermore, we show that the silencing of CANX in APC diminishes their capacity to activate antigen-specific CD4⁺ T cells. Remarkably, using co-immunoprecipitation followed by mass spectrometry, we identified CANX as a binding partner of T6BP, among 116 high-confidence T6BP proximal proteins. T6BP and CANX interaction was confirmed in HeLa-CIITA as well as in B cells and DC, strongly suggesting that our observations are not limited to our model APCs.

It has been proposed that the ER distribution of CANX might determine its functions as a chaperone involved in protein quality control or in the regulation of Ca²⁺ transfer to mitochondria (Lynes *et al*, 2013). Several post-translational modifications influence both the cellular distribution and the functions of calnexin: phosphorylation of the cytosolic tail of CANX leads to a redistribution from peripheral ER tubules to a juxtannuclear ER (Myhill *et al*, 2008) while palmitoylation of the tail seems to assign specific tasks to calnexin within the ER, in particular, a role in protein folding (Lynes *et al*, 2013) and a localization at the proximity of the ribosome complexes (Lakkaraju *et al*, 2012). We show here that T6BP binds to the cytosolic tail of CANX. To our knowledge, there is no published evidence that CANX is ubiquitinated on its cytosolic tail, but we believe this possibility should be investigated further as T6BP might use its Ub-binding domain to bind to CANX, providing a molecular link between T6BP and CANX functions in the formation of MHC-II

loading complexes and thus antigen presentation. Note that CANX has also been shown to contribute to the assembly of MHC-I molecules by protecting free MHC-I molecules from degradation (Vassilakos *et al*, 1996) and by binding to the TAP-tapasin complex (Diedrich *et al*, 2001). However, CANX action on MHC-I molecule assembly and transport to the cell surface seem dispensable (Scott & Dawson, 1995; Prasad *et al*, 1998), which would explain the lack of influence of CANX on the MHC-I immunopeptidome, in the absence of T6BP.

We suggest here that CANX is a key factor involved in T6BP-mediated regulation of MHC-II loading that strongly influences the repertoire and affinity of presented peptides. However, we do not exclude that other cellular factors or pathways also participate in T6BP action on MHC-II molecules. Jongsma *et al* showed that the ER ubiquitin ligase RNF26 interacts with p62 (SQSTM1) and that it employs a ubiquitin-based communication with Tollip, T6BP, or EPS15 to cluster recycling, early and late endosomes in so-called perinuclear clouds. In the model, deubiquitination of p62 by the DUB UPS15 leads to the release of the vesicles for maturation (Jongsma *et al*, 2016). The authors showed that the silencing of RNF26 leads to the dispersion of EEA1⁺ and CD63⁺ vesicles, in the cytoplasm of the cells. They also show that the silencing of T6BP has a broad influence on the shape of cells and leads to the dispersion of the cloud of CD63⁺ vesicles. Our observations also highlight that T6BP-silencing influences CD63⁺ vesicles; however, our results indicate that CD63⁺ vesicles are maintained in the perinuclear region. We confirmed these observations using lysotracker and LAMP-1 markers of acidified and late endosomes, respectively. The different behavior of CD63⁺ vesicles in siT6BP-treated cells might be due to the expression of the HLA locus driven by CIITA, in our model of APCs. Nonetheless, our work confirms the involvement of T6BP in the traffic of endosomes. In addition, we found, in the interactome study of T6BP, the DUB UPS15. Interestingly, although T6BP affects EEA1⁺ early endosomes perinuclear localization, we excluded the possibility that the effect of T6BP on MHC-II-restricted antigen presentation relies on early endosomal defect since EEA1⁺ vesicles do not contain MHC-II molecules in our APCs. Overall, we show that T6BP impacts the trafficking of MHC-II-rich compartments that bear hallmarks of the MIIC, namely HLA-DM, CD63⁺, and LAMP-1. More globally T6BP-silencing seems to affect the cellular localization of acidified vesicular compartments corresponding to late endosomes, lysosomes, and as already demonstrated autophagosomes (Petkova *et al*, 2017), without significantly reducing the expression levels of the various markers. Accumulating evidence suggests that the positioning of intracellular vesicles controls their functions (Neeffjes *et al*, 2017) and intravesicular pH in particular (Johnson *et al*, 2016). The repositioning of the MIIC mediated by T6BP could influence the activation of intravesicular pH-dependent proteases that participate in the cleavage of CD74 and antigen processing. In this regard, it is interesting to note that we identified in the interactome of T6BP, ATP6V0A1 a subunit of the vATPase that plays a critical role in mediating vesicular acidification (Forgac, 2007). On the other hand, CD74 has been shown to play, by itself, a role in endosomal membrane trafficking (Romagnoli *et al*, 1993; Margiotta *et al*, 2020) and perhaps in proteolysis of antigens (Schröder, 2016). It was recently reported that the CD74 p41 isoform interacts with cathepsins and regulates their activity in endosomes (Bruchez *et al*, 2020). These studies and others suggest

that CD74 might exert various functions not limited to its canonical role in antigen presentation and as a chaperone (Schröder, 2016). Thereafter, the modifications in late endosomes/lysosomes positioning and of the MHC-II immunopeptidome in T6BP-silenced cells could be an indirect consequence of CD74 degradation.

Our interactome also revealed as candidate partners for T6BP, the HLA-A, -C, -DQ α 1, and -DR β 1 molecules. Interestingly, the cellular distribution of both HLA class I and II molecules is regulated by the addition of ubiquitin (Ub) moieties (De Angelis Rigotti *et al*, 2017; Shin *et al*, 2006; Walseng *et al*, 2010). In the case of HLA-DR, ubiquitination of the lysine residue (K235) of HLA-DR β 1 plays a major role in regulating the cellular localisation of mature HLA-DR molecules (Lapaque *et al*, 2009). Although T6BP has the capacity to bind ubiquitinated proteins, we favor the hypothesis that T6BP and HLA molecules might be part of larger molecular complexes or lipid compartments in particular since we observed neither a co-localization of T6BP with HLA-DR molecules nor a significant difference in the kinetics of HLA-DR endocytosis in HeLa-CIITA cells silenced for T6BP expression.

The autophagy receptor T6BP as well as OPTN, NDP52, p62, and NBR1 harbor Ub- and LC3-binding motifs, whose functions are well characterized in selective autophagy (Kirkin & Rogov, 2019). In addition, T6BP and NDP52 share a N-terminal SKIP carboxyl homology (SKICH) domain target of TANK-binding kinase-1 (TBK1) phosphorylation that acts as an upstream regulator of mitophagy (Fu *et al*, 2018). Beyond selective autophagy, ARs also modulate the traffic and maturation of autophagosomes and endosomes. The Ub-binding domains of T6BP, OPTN, and p62 have been implicated in regulating the NF- κ B pathway where together with A20 they down-modulate the activation of this pathway during inflammation (Weil *et al*, 2018). T6BP, NDP52, and OPTN also bind to myosin-VI, which recruits Tom-1-expressing endosomes and lysosomes, facilitating autophagosome maturation in lytic vesicles (Sahlender *et al*, 2005; Morriswood *et al*, 2007; Tumbarello *et al*, 2012). Recent work suggested that Ub and myosin-VI compete for the binding to T6BP (Hu *et al*, 2018). In T6BP's interactome, we identified known protein partners of T6BP involved for instance in NF- κ B signaling pathways (e.g., TBK1, TRAF2, ITC, SQSTM1/p62). However, other described T6BP partners such as myosin-VI were not identified, likely reflecting that T6BP interactions occur in a cell type-specific manner (O'Loughlin *et al*, 2018). Nonetheless, we revealed novel potential partners of T6BP involved in the ubiquitin/proteasome (e.g., E3 Ub-ligases UBR1, 2 and 4), the UPR/protein folding (e.g., BAG6, EIF2 α , calnexin), endocytosis (e.g., COPB1), and antigen presentation pathways (e.g., HLA molecules). We also found that T6BP interacts with NBR1 that has been found together with p62 in larger protein complexes and ubiquitinated protein aggregates (Weil *et al*, 2018). Much remains to be learned on the molecular mechanisms and motifs involved in the variety of T6BP molecular interactions and functions, in particular in MHC-II antigen presentation that we unravel here. Side-by-side comparison of AR functional domains will most likely bring new insights.

Our work reveals that T6BP regulates the cellular positioning of the MHC-II loading compartment and the stability of CD74, through an interaction with CANX, and exerts a direct influence on MHC-II-restricted antigen presentation. This novel role of T6BP in the activation of adaptive antiviral immunity further highlights the diverse nonredundant functions exerted by autophagy receptors.

Materials and Methods

Cells

The HeLa-CIITA cells (homozygotes for HLA-DR β 1*0102 allele), the B (DG-75), and the dendritic-like cell lines (KG-1) were kindly provided by Philippe Benaroch (Institut Curie, Paris, France), Hugo Mouquet (Institut Pasteur, France) and Peter Cresswell (Yale University School of Medicine, USA), respectively. Cells were cultured with RPMI GlutaMax 1640 (Gibco) complemented with 10% FBS (Dutscher), 1% penicillin/streptomycin, and 50 μ g/mL Hygromycin B (Thermo Fisher) only for HeLa-CIITA cells.

HIV-1- & HCMV-specific CD4⁺ T cell clones

Gag-specific CD4⁺ T cell clones (F12) are specific for HIV Gag-p24 (gag2: aa 271–290) and restricted by HLA-DR β 1*01 as previously described (Moris *et al*, 2006; Coulon *et al*, 2016). HCMV-specific CD4⁺ T cell clones are specific for HCMV pp65 antigen (pp65: aa 108–127) and restricted by HLA-DR β 1*01. Pp65-specific clones were isolated from PBMCs of healthy donors after several rounds of *in vitro* stimulation with synthetic peptide corresponding to immunodominant epitopes from the pp65 protein. Pp65-specific cells were isolated using the IFN γ secreting assay from Miltenyi Biotec and cloned by limiting dilution. F12 and pp65 clones were restimulated and expanded, as previously described (Moris *et al*, 2006), using irradiated feeders and autologous or HLA-matched lymphoblastoid cell lines loaded with cognate peptides in T cell cloning medium: RPMI 1640 containing 5% human AB serum (Institut Jacques Boy), recombinant human IL-2 (100 IU/ml, Miltenyi Biotec), PHA (0,25 μ g/ml, Remel), nonessential amino acids, and sodium pyruvate (both from Life Technologies). At least 1 h before co-culture with HeLa-CIITA cells, T cell clones were thawed and allowed to rest at 37°C in RPMI containing DNase (5 μ g/mL, New England Biolabs).

Viral antigens and plasmids

The pTRIP-CMV-Gag (a kind of gift from Nicolas Manel, Institut Curie, Paris, France), pGag-LC3, and Gag-LC3_{G120A} plasmids were already described (Coulon *et al*, 2016). The pp65 encoding cDNA (a kind of gift from Xavier Saulquin, Université de Nantes, Nantes) was cloned in the lentiviral vector cppT-EF1 α -IRES-GFP. The GFP-T6BP encoding plasmid is a kind of gift from Folma Buss (University of Cambridge, UK) (Tumbarello *et al*, 2015).

Cell transfections

HeLa-CIITA cells were incubated in 6-well plates using 2–4.10⁵ cells/well using OPTIMEM (Gibco) complemented with 10% FBS and 1% penicillin/streptomycin. Twenty-four hours later, cells were transfected with 40 pmol of siRNA targeting NDP52 (L-010637-00-0005), OPTN (L-016269-00-0005), p62 (L-010230-00-0005), T6BP (L-016892-00-0020 Dharmacon) or SI02781296, Qiagen), CANX (SI02663367 and SI02757300, Qiagen) or a scrambled siRNA as control (D-001810-10-20, Dharmacon), using Lipofectamine RNAiMax (13778–150, Thermo Fisher) as transfection reagent. After 24 h of transfection, cells were transfected with the cDNA encoding the

viral antigens (1 μ g per well of a 6-well plate) using Viromer RED (Lipocalyx) and following manufacturer instructions. Twenty-four hours later, Gag and pp65 expressions were assessed using anti-Gag antibody (KC57-RD1, Beckman-Coulter) and anti-pp65 antibody (mouse, Argene) combined with goat anti-mouse antibody (AF488, Thermo Fisher), respectively.

Flow cytometry

Cell viability was evaluated using LIVE/DEAD (Thermo Fisher) or Zombie (Biolegend) and the following antibodies were used: HLA-DR-specific L243 and T \ddot{U} 36 (both in-house and kindly provided by Philippe Benaroch, Institut Curie, Paris) and goat anti-mouse (AF488, Thermo Fisher). Forty-eight hours after siRNA transfection, cell-surface staining assays were performed using standard procedures (30 min, 4°C). HIV-Gag and HCMVpp65 production was detected using intracellular staining. Briefly, cells were fixed with 4% PFA (10 min, RT), washed, and permeabilized with PBS containing 0.5% BSA and 0.05% Saponin, prior to antibody staining. Samples were processed on Fortessa cytometer using FACSDiva software (BD Biosciences) and further analyzed using FlowJo2 software (Tree Star).

IFN γ ELISPOT assay

ELISPOT plates (MSIPN4550, Millipore) were prewet and washed with PBS, and coated overnight at 4°C with anti-IFN γ antibody (1-DIK, Mabtech). Plates were washed using PBS and then saturated with RPMI complemented with 10% FBS. Plates were washed and HeLa-CIITA cells (10⁵ cells/well) were co-cultured with T cell clones (5.10³ and 1.10³ cells/well) overnight at 37°C. Cells were removed and plates were then washed with PBS-0,05% Tween-20 prior to incubation with biotinylated anti-IFN γ antibody (7-B6-1, Mabtech) (2 h, RT). Spots were revealed using alkaline-phosphatase coupled to streptavidin (0,5 U/ml, Roche Diagnostics) (1 h, RT) and BCIP/NBT substrate (B1911, Sigma-Aldrich) (30 min, RT). Reactions were stopped using water. A number of spots were counted using AID reader (Autoimmun Diagnostika GmbH). For each experimental condition, ELISPOTs were performed mostly in triplicates or at least in duplicates.

Western Blotting

Forty-eight hours after siRNA transfection, 10⁶ HeLa-CIITA cells were washed in cold PBS and lysed in 100–300 μ l of lysis buffer (30 min, 4°C), mixing every 10 min. When stated, cells were pretreated with chloroquine (50 μ M, 16 h) or epoxomicin (50 nM, 16 h). Depending on the experiments, three different lysis buffers were used: 1- PBS containing 1% Nonidet P-40; 2–50 mM Tris–HCl pH 7.5 containing 100 mM NaCl, 1% Triton X-100, 0.5 mM EGTA, 5 mM MgCl, 2 mM ATP; 3–50 mM Tris–HCl pH 7.5 containing 150 mM NaCl, 1% IGEPAL, 0.5 mM EDTA, 5 mM MgCl, all three supplemented with 1x protease inhibitor (Roche). Cell lysates were then centrifuged at 20,000 g (10 min, 4°C), supernatants harvested and mixed with Sample Buffer (NuPAGE, Invitrogen) and Sample Reducing Agent (NuPAGE, Invitrogen) and denatured (5 min, 95°C). Denatured samples were analyzed by SDS gel electrophoresis using 4–12% Bis-Tris gels (NuPAGE, Invitrogen), transferred to a nitrocellulose membrane

(NuPAGE, Invitrogen), and immunoblotted. Anti-T6BP (HPA024432, Sigma-Aldrich), anti-NDP52 (HPA023195, Sigma-Aldrich), anti-CANX (PA5-34754, Thermo Fisher), anti-PTN (ab23666, Abcam), anti-p62 (sc-28,359, Santa Cruz Biotechnology), anti-HLA-DR (TAL1B5, Invitrogen), anti-LC3 (M152, MBL International), anti-actin (3700S, Cell Signaling Technology), anti-tubulin (2148S, Cell Signaling Technology), anti-CD74 (ab22603, Abcam or VIC-Y1, 14-0747-82, Thermo Fisher), anti-GFP (11,814,460,001, Roche), anti-ubiquitin (eBioP4D1, Thermo Fisher), goat anti-mouse (Sigma-Aldrich) and goat anti-rabbit both coupled to HRP (Abcam) antibodies were used according to manufacturer instructions. Blots were revealed using Pierce ECL Plus Substrate (Invitrogen) and chemiluminescence analyzed using ImageQuant LAS 4000.

Confocal microscopy

Forty-eight hours after siRNA transfections, HeLa-CIITA cells were plated on glass coverslips and then fixed with 4% PFA (10 min, RT). Cells were washed 3 times with PBS, saturated with goat or donkey serum, and permeabilized with PBS containing 0.5% BSA and 0.05% Saponin (1 h, RT). Cells were washed with PBS and incubated (OVN, 4°C) with primary antibodies: L243 or TÛ36 (both in-house and kindly provided by P. Benaroch, Institut Curie, Paris), rabbit anti-HLA-DR (a kind gift from Jacques Neefjes, Leiden University, the Netherlands), anti-LAMP-1 (H4A3, DSHB), anti-CD63 (MA-18149), anti-CD74 (14-0747-82) all from Thermo Fisher, anti-EEA1 (C45B10, Cell signaling), anti-T6BP (HPA024432, Sigma-Aldrich), anti-HLA-DM (sc-32,248, Santa Cruz) and Lysotracker (Deep Red, L12492). Cells were incubated with species-specific antibodies: goat anti-mouse coupled to Alexa Fluor 488 or Alexa Fluor 405 (Thermo Fisher), donkey anti-rabbit coupled to Alexa 546 (A10040, Invitrogen) in PBS containing 0.5% BSA and 0.05% Saponin (1 h, RT). When required sequential stainings were performed. Nuclei were stained with DAPI (17,507, AAT Bioquest). After washing with PBS, samples were mounted on glass slides with Dako fluorescence mounting medium. Samples were imaged using a laser scanning confocal microscope with 63X, NA 1.3 oil immersion objective. The number of vesicles, the intensity, and the distances of each vesicle to nucleus were quantified using an in-house ImageJ Python script (developed by Aziz Fouché, ENS Paris-Saclay, Paris). Potential co-localizations were determined using the object-based co-localization method JACoP (Just Another Co-localization Plugin) and coloc2 (Pearson's coefficient) of the ImageJ software, for punctuated/vesicular and cytosolic/diffuse staining, respectively. For the Proximity ligation assay (PLA), 48 h after siRNA transfections, HeLa-CIITA cells, cultured overnight on coverslips, were fixed with 4% PFA (10 min, RT), washed 3x with PBS, and treated with 50 mM NH4Cl (15 min, RT) prior incubation with anti-T6BP (Rabbit, 1:200, HPA024432) and anti-CANX (Mouse, 1:500, MA3-027, Thermo Fisher scientific) in PBS containing 1%, BSA and 0.1% Saponin (1 h, RT). PLA secondary probes (DUO92002, DUO92004) were then used according to the manufacturer's instructions (Sigma-Aldrich). Briefly, 40 µl (1:5 dilution) of the PLA was added (37 °C, 60 min) and washed with buffer A (DUO82049, Sigma-Aldrich). 40 µl of the ligation mix (DUO92014, Sigma-Aldrich) was then applied to each of the coverslips to complete the ligation process (30 min, 37 °C). Coverslips were then incubated with 40 µl polymerization mix (100 min, 37 °C) and washed. Coverslips were

mounted on slides with Fluoromount G (Thermo Fisher). Images were acquired using an SP8 confocal microscope and dots were counted using the find maxima plugin in Fiji software.

Reverse transcription-quantitative polymerase chain reaction (RT-qPCR)

Total cellular RNA was isolated using RNeasy kit (Qiagen, Valencia, CA). RNA concentrations were determined by spectrophotometry at 260 nm. The relative level of CD74 and T6BP mRNAs was determined using the comparative Cq method. Actin was used as endogenous control. The primers and probes used for quantitation of CD74, T6BP, and actin were designed by Olfert Landt and purchased from TIB MolBiol. Sequences are listed in Appendix Table S1. The RT-qPCRs were performed in a Light Cycler 1.5 instrument in capillaries using a final volume of 20 µl. The reactions were performed using 300 nM specific sense primer, 300 nM specific antisense primer, 200 nM specific TaqMan probe (TM), and the LightCycler® Multiplex RNAVirus Master mix (ROCHE). The programs were: reverse transcription at 55°C for 10 min, initial denaturation at 95°C for 5 min followed by 45 cycles of amplification. For CD74 and T6BP cycles were: 95°C for 5 s, 60°C for 15 s + fluorescence measurement, and 72°C for 5 s. For actin cycles were: 95°C for 20s, 67°C for 30s + fluorescence measurement, and 72°C for 5 s.

Pulse-Chase experiment

48 h post-siRNA transfection HeLa-CIITA cells were preincubated in Met/Cys-free RPMI 1640 medium containing 1% penicillin/streptomycin, 1% glutamine, and 10% dialyzed FCS for 1 h. Cells (five million) were then pulsed for 30 min with 0.5 mCi of ³⁵S-Met/Cys (ICN) and chased in an unlabelled medium supplemented with 5 mM cold methionine. Cells were collected at the indicated time points and then lysed in a buffer containing 20 mM Tris-HCl (pH 7.5), 150 mM NaCl, 2 mM MgCl₂, 1% Triton X-100, and an inhibitor cocktail (Roche). Each sample was normalized for the protein concentration. Lysates were precleared with mouse serum, and MHC class II/li complexes were immunoprecipitated with the TÛ36 antibody and/or reimmunoprecipitated with VICY1 antibody (14-0747-82, Thermo Fisher). Samples were boiled (95°C) or unboiled (room temperature) in SDS loading buffer and separated on 12% SDS-PAGE (Novex). Quantification of the results was made using a phosphoimager (Fuji).

Electron Microscopy

HeLa-CIITA cells (2.10⁵ cells/well) were cultured on glass coverslips in 6-well plates. 24 h later, cells were transfected as described with siRNA control or targeting T6BP, cells were cultured for 48 h and fixed with 2.5% glutaraldehyde, 1% PFA for 1 h at room temperature. The coverslips were washed 3 times with 0.2 M phosphate buffer pH 7.4, followed by a 1-h incubation in 1% osmium, and 1.5% ferrocyanide of potassium. After 3 washes in water, the coverslips were successively treated with 50%, 70%, 90%, 100%, and 100% Ethanol for 10 min each. The coverslips were then incubated for 2 h on 50% epoxy in ethanol, followed by 2 h in pure epoxy, and finally in pure epoxy overnight for polymerization at 60°C. Ultrathin (70 nm) sections were cut using a diamond knife (45°

angle) on a Leica UC6 ultramicrotome. Sections were collected on Formvar™ carbon-coated copper grids. Some sections were stained with uranyl acetate at 2% (Merk) for 15 min and lead citrate (Agar) and washed three times with milliQ water and dried at room temperature. Observations were performed with a JEOL JEM-1400 transmission electron microscope operating at 120 kV. Images were acquired using a postcolumn high-resolution (9 10⁶ pixels) camera (Rio9; Gatan) and processed with Digital Micrograph (Gatan) and ImageJ.

Immunoepitidome

Isolation of HLA ligands

HLA class I and II molecules of HeLa-CIITA cells were isolated using standard immunoaffinity purification (Falk *et al*, 1991; Nelde *et al*, 2019). Snap-frozen samples were lysed in 10 mM CHAPS/PBS (AppliChem, Gibco) with 1x protease inhibitor (Roche). HLA class I- and II-associated peptides were isolated using the pan-HLA class I-specific mAb W6/32 and the pan-HLA class II-specific mAb TÛ39 (both in-house mouse monoclonal) covalently linked to CNBr-activated Sepharose (GE Healthcare). HLA-peptide complexes were eluted by repeated addition of 0.2% TFA (trifluoroacetic acid, Merck). Eluted HLA ligands were purified by ultrafiltration using centrifugal filter units (Millipore). Peptides were desalted using ZipTip C18 pipette tips (Millipore), eluted in 35 µl 80% acetonitrile (Merck)/0.2% TFA, vacuum-centrifuged and resuspended in 25 µl of 1% acetonitrile/0.05% TFA and samples stored at -20 °C until LC-MS/MS analysis.

Analysis of HLA ligands by LC-MS/MS

Isolated peptides were separated by reversed-phase liquid chromatography (nano-UHPLC, UltiMate 3,000 RSLCnano; ThermoFisher) and analyzed in an online-coupled Orbitrap Fusion Lumos mass spectrometer (Thermo Fisher). Samples were analyzed in five technical replicates, and sample shares of 20% were trapped on a 75 µm × 2 cm trapping column (Acclaim PepMap RSLC; Thermo Fisher) at 4 µl/min for 5.75 min. Peptide separation was performed at 50 °C and a flow rate of 175 nl/min on a 50 µm × 25 cm separation column (Acclaim PepMap RSLC; Thermo Fisher) applying a gradient ranging from 2.4 to 32.0% of acetonitrile over the course of 90 min. Samples were analyzed on the Orbitrap Fusion Lumos implementing a top-speed CID method with survey scans at 120 k resolution and fragment detection in the Orbitrap (OTMS2) at 60 k resolution. The mass range was limited to 400–650 m/z with precursors of charge states 2+ and 3+ eligible for fragmentation.

Database search and spectral annotation

LC-MS/MS results were processed using Proteome Discoverer (v.1.3; Thermo Fisher) to perform a database search using the Sequest search engine (Thermo Fisher) and the human proteome as reference database annotated by the UniProtKB/Swiss-Prot. The search-combined data of five technical replicates was not restricted by enzymatic specificity, and oxidation of methionine residues was allowed as a dynamic modification. Precursor mass tolerance was set to 5 ppm, and fragment mass tolerance to 0.02 Da. The false discovery rate (FDR) was estimated using the Percolator node (Käll *et al*, 2007) and was limited to 5%. For HLA class I ligands, peptide lengths were limited to 8–12 amino acids. For HLA class II, peptides

were limited to 12–25 amino acids in length. HLA class I annotation was performed using NetMHCpan 4.0 (Jurtz *et al*, 2017) annotating peptides with percentile rank below 2% as previously described (Ghosh *et al*, 2019).

For HLA class II peptides, the Peptide Landscape Antigenic Epitope Alignment Utility (PLAtEAU) algorithm (Alvaro-Benito *et al*, 2018) was used to identify and to estimate the relative abundance of the core epitopes based on the LC-MS/MS intensities. The results are presented as Volcano plots using Perseus software (Tyanova *et al*, 2016). The relative affinities of the core epitope to HLA-DRβ1*0102, expressed by HeLa-CIITA cells, were estimated using NetMHCIIpan 4.0 (Reynisson *et al*, 2020).

Interactome

Co-immunoprecipitation

HeLa-CIITA cells were harvested 24 h after cDNA transfection with either plasmid encoding GFP-T6BP (kind gift from F.Buss, Cambridge, UK) or encoding GFP. 2.10⁷ cells were washed in cold PBS and lysed in 300 µl of lysis buffer (50 mM Tris-HCl pH 7.5, 100 mM NaCl, 1% Triton X-100, 0.5 mM EGTA, 5 mM MgCl, 2 mM ATP, and 1x protease inhibitor; Roche; 30 min, ice), mixing every 10 min and centrifuged at 20,000 g (20 min, 4°C). Lysates were recovered, 300 µl of wash buffer (50 mM Tris-HCl pH 7.5, 150 mM NaCl, 0.5 mM EDTA) was added and the pellets were discarded. GFP-Trap agarose magnetic beads (Chromotek) were vortexed, and 25 µl of bead slurry was washed 3 times with cold wash buffer. Each diluted lysate was added to 25 µl of equilibrated beads and tumbled end-over-end (1 h, 4°C). Beads were collected using a magnetic support and washed 3 times. For Western Blot analysis, SDS-sample buffer was added to aliquots and the samples were boiled (5 min, 99°C).

On-bead digestion for mass spectrometry

Following immunoprecipitation with GFP-Trap (Chromotek), digestions were performed using manufacturer instructions on the P3S proteomic core facility of Sorbonne Université. For each sample, beads were resuspended in 25 µl of elution buffer I (50 mM Tris-HCl pH 7.5, 2 M urea, 5 µg/ml sequencing grade Trypsine, 1 mM DTT) and incubated in a thermomixer at 400 rpm (30 min, 30°C). Beads were collected using a magnetic support and the supernatants were recovered. For elution, beads were then washed with 50 µl of elution buffer II (50 mM Tris-HCl pH 7.5, 2 M urea, 5 mM iodoacetamide) and collected with a magnetic support. Supernatants were harvested and mixed with the previous ones. This elution was repeated once. Combined supernatants were incubated in a thermomixer at 400 rpm (overnight, 32°C). Reactions were stopped by adding 1 µl trifluoroacetic acid and digests were desalted using homemade StageTips. StageTips were first rehydrated with 100 µl of methanol and then equilibrated with 100 µl of 50% acetonitrile and 0.5% acetic acid. After peptide loading, StageTips were washed with 200 µl of 0.5% acetic acid, and peptides were eluted with 60 µl of 80% acetonitrile 0.5% acetic acid. Eluted peptides were totally dried using a SpeedVac vacuum concentrator (Thermo), solubilized in 20 µl of 2% acetonitrile 0.1% formic acid before LC-MS/MS analysis.

LC-MS/MS

Peptide mixtures were analyzed with a nanoElute UHPLC (Bruker) coupled to a timsTOF Pro mass spectrometer (Bruker). Peptides

were separated on an Aurora RP-C18 analytical column (25 cm, 75 μ m i.d., 120 \AA , 1,6 μ m IonOpticks) at a flow rate of 300 nL/min, at 40°C, with mobile phase A (ACN 2% / FA 0.1%) and B (ACN 99.9% / FA 0.1%). A 30 min elution gradient was run from 0% to 3% B in 1 min, 3% to 15% B in 17 min then 15% to 23% B in 7 min and 23% to 32% B in 5 min. MS acquisition was run in DDA mode with PASEF. Accumulation time was set to 100 msec in the TIMS tunnel. The capillary voltage was set to 1,6 kV, mass range from 100 to 1700 m/z in MS and MS/MS. Dynamic exclusion was activated for ions within 0.015 m/z and 0.015 V.s/cm² and released after 0,4 min. The exclusion was reconsidered if precursor ion intensity was 4 times superior. Low abundance precursors below the target value of 20,000 a.u and intensity of 2,500 a.u. were selected several times for PASEF-MS/MS until the target value was reached. Parent ion selection was achieved by using a two-dimensional m/z and 1/k0 selection area filter allowing the exclusion of singly charged ions. Total cycle time was 1,29 s with 10 PASEF cycles.

Data Analysis

Raw data were processed with MaxQuant version 1.6.5.0, with no normalization, no matching between runs, and a minimum of 2 peptide ratios for protein quantification. The output protein file was filtered with ProStar 1.14 to keep only proteins detected in 2 samples or more in at least 1 of the 2 conditions. Missing values were imputed using SLSA (Structured Least Square Adaptive) algorithm for partially missing values in each condition and DetQuantile algorithm for missing values in an entire condition. In order to select relevant binding partners, data were statistically processed using the limma test and filtered to retain only differentially expressed preys (FDR 1%) with a fold change \geq 10 between T6BP-GFP and GFP conditions. Selected preys were uploaded to the CRAPome v2 (Contaminant Repository for Affinity Purification) online analysis tool to identify potential contaminants. For each binding partners, a Significance Analysis of INteractome (SAINT) probability threshold was assessed by the Resource for Evaluation of Protein Interaction Networks (REPRINT) using the default settings. Selected preys were then uploaded in Ingenuity Pathway Analysis software version 49,932,394 (QIAGEN Inc.) to perform annotation and over-representation analysis. Finally, network visualization was designed using Cytoscape software (v. 3.7.1).

Co-immunoprecipitation: CANX / T6BP / GST-TM-cytoTail

HeLa-CIITA cells were harvested, counted, and lysed in two different buffers depending on the experiments: 1- m-RIPA buffer (1% NP40, 1% sodium deoxycholate, 150 mM NaCl, 50 mM Tris-pH 7.5; 2- NP-40 lysis buffer, 50 mM Tris-HCl pH 7.5 containing 150 mM NaCl, 1% IGEPAL, 0.5 mM EDTA, 5 mM MgCl), both supplemented with complete protease inhibitors (Roche, Basel, Switzerland). CANX and T6BP were immunoprecipitated using anti-CANX antibody PA5-34754 (Invitrogen) coupled to protein A Sepharose magnetic beads (Ademtech 0423) and anti-TAX1BP1 antibody HPA024432 (Sigma-Aldrich) together with protein A Sepharose (GE Healthcare), respectively. The GST-TM-cytoTail nucleotide sequence was synthesized and cloned into pLV-EF1a-IRES-Puro by GeneCust. pLV-EF1a-IRES-Puro was a gift from Tobias

Meyer (Addgene plasmid # 85132; <http://n2t.net/addgene:85132>; RRID:Addgene_85132) (Hayer *et al*, 2016). GST-TM-cytoTail sequence contains the following sequence: CANX leader, GST, a short fragment of the ER luminal domain of CANX, CANX TM, CANX cytosolic tail; and is: ATGGAAGGGAAGTGGTTGCTGTG-TATGTTACTGGTGGCTTGGAACTGCTATTGTTGAGGCTCCCTATA CTAGGTTATTGAAAATTAAGGGCCTTGCAACCCACTCGACTTC TTTTGAATATCTTGAAGAAAAATATGAAGAGCATTGTATGAGC GCGATGAAGGTGATAAATGGCGAAACAAAAGTTTGAATTGGGTT TGGAGTTTCCAATCTTCTTATTATATGATGGTGATGTTAAATT AACACAGTCTATGGCCATCATACGTTATATAGCTGACAAGCACAAC ATGTTGGGTTGTTGCCAAAAGAGCGTGCAGAGATTTCAATGCTTG AAGGAGCGGTTTTGGATATTAGATACGGTGTTCGAGAATTGCATA TAGTAAAGACTTTGAAACTCTCAAAGTTGATTTTCTTAGCAAGCTA CCTGAAATGCTGAAAATGTTGCAAGATCGTTTATGTCATAAAACAT ATTTAAATGGTGATCATGTAACCCATCCTGACTTCATGTTGTATGA CGCTCTTGATGTTGTTTTATACATGGACCAATGTGCCTGGATGCGT TCCAAAATTAGTTGTTTTAAAAAACGTATTGAAGCTATCCACA AATTGATAAGTACTTGAATCCAGCAAGTATATAGCATGGCCTTTG CAGGGCTGGCAAGCCACGTTTGGTGGTGGCGACCATCTCCAAAAA AGAAAGCTGCTGATGGGGCTGCTGACCCAGGCGTTGTGGGGCAGA TGATCGAGGCAGCTGAAGAGCGCCGAAGAAAGCTGCTGATGGGG CTGCTGAGCCAGGCGTTGTGGGGCAGATGATCGAGGCAGCTGAAG AGCGCCCGTGCTGTGGGTAGTCTATATTCTAACTGTAGCCCTTCC TGTGTTCTCGTTATCTCTTCTGCTGTTCTGGAAAGAAACAGACC AGTGGTATGGAGTATAAGAAAAGTATGCACCTCAACCGGATGTGA AGGAAGAGGAAGAAGAGAAGGAAGAGGAAAAGGACAAGGGAGAT GAGGAGGAGGAAGGAGAAGAGAAAAGTGAAGAGAAAACAGAAAAG TGATGCTGAAGAAGATGGTGGCACTGTCAGTCAAGAGGAGGAAGA CAGAAAACCTAAAGCAGAGGAGGATGAAATTTTGAACAGATCACCA AGAAACAGAAAGCCACGAAGAGAGTGA. HeLa-CIITA cells were transfected with GST-TM-cytoTail construct or the vector not encoding TM-cytoTail. 24 h post-transfection, cells were harvested and lysed using NP40 lysis buffer (10 mM Tris-HCl pH 7.5, 150 mM NaCl, 0,5 mM EDTA, 0,5% IGEPAL). The GST-immunoprecipitation was performed using GST-Trap Agarose from Chromotek. The immunoprecipitation (IP) fractions were extensively washed (at least 3 times) in NP40 lysis buffer. The input, the flow-through, and the IP fractions were analyzed by SDS-PAGE and the proteins revealed using Western blot.

Statistical analysis

Statistical significances (*P*-values) were calculated using Prism Software (GraphPad).

Data availability

The mass spectrometry proteomics data have been deposited to the ProteomeXchange Consortium (<http://proteomecentral.proteomexchange.org>) via the PRIDE (Perez-Riverol *et al*, 2019) partner repository with the dataset identifier PXD024330 and PXD024417 for the T6BP-interactome and HeLa-CIITA immunopeptidome, respectively: <http://www.ebi.ac.uk/pride/archive/projects/PXD024330>; <http://www.ebi.ac.uk/pride/archive/projects/PXD024417>

Expanded View for this article is available [online](#).

Acknowledgements

This work was granted by the ANR project AutoVirim (ANR-14-CE14-0022). We thank the “P3S” core facility of Sorbonne University for its expertise. The present work has benefited from the Imagerie facility of Imagerie-Gif, (<http://www.i2bc.paris-saclay.fr>), member of IBISA (<http://www.ibisa.net>), supported by l'Agence Nationale de la Recherche (ANR-11-EQPX-0029/Morphoscope), “France-BioImaging” (ANR-10-INSB-04-01) and the Labex “Saclay Plant Science” (ANR-11-IDEX-0003-02). C.R. and M.P. were supported by AutoVirim. We thank the Dormeur Foundation, Vaduz, for providing the AID ELISPOT Reader. We also thank the Agence Nationale de Recherche sur le SIDA et les hépatites virales (ANRS) and Sidaction for funding. M.P. and L.B. were supported by Sidaction. A.K. and R.J.-M. were ANRS fellows.

Author contributions

Gabriela Sarango: Formal analysis; investigation; methodology; writing—review and editing. **Clémence Richetta:** Formal analysis; validation; investigation; methodology; writing—original draft; writing—review and editing. **Mathias Pereira:** Formal analysis; investigation; methodology; writing—original draft; writing—review and editing. **Anita Kumari:** Formal analysis; investigation; methodology; writing—review and editing. **Michael Ghosh:** Data curation; formal analysis; investigation; methodology. **Lisa Bertrand:** Investigation; methodology. **Cédric Pionneau:** Data curation; formal analysis; investigation; methodology; writing—review and editing. **Morgane Le Gall:** Data curation; software; formal analysis. **Sylvie Grégoire:** Investigation; methodology. **Raphaël Jeger-Madiot:** Investigation; methodology. **Elina Rosoy:** Investigation; methodology. **Frédéric Subra:** Supervision; validation; investigation; methodology. **Olivier Delelis:** Formal analysis; supervision; validation; investigation; methodology. **Mathias Faure:** Resources; funding acquisition. **Audrey Esclatine:** Resources; funding acquisition. **Stéphanie Graff-Dubois:** Supervision; investigation; methodology. **Stefan Stevanović:** Data curation; formal analysis; validation; investigation; methodology. **Bénédicte Manoury:** Conceptualization; formal analysis; supervision; validation; investigation; methodology; writing—review and editing. **Bertha Cecilia Ramirez:** Formal analysis; supervision; validation; investigation; methodology; writing—review and editing. **Arnaud Moris:** Conceptualization; resources; formal analysis; supervision; funding acquisition; validation; investigation; visualization; methodology; writing—original draft; project administration; writing—review and editing.

Disclosure and competing interests statement

The authors declare that they have no conflict of interest.

References

- Aichinger M, Wu C, Nedjic J, Klein L (2013) Macroautophagy substrates are loaded onto MHC class II of medullary thymic epithelial cells for central tolerance. *J Exp Med* 210: 287–300
- Alvaro-Benito M, Morrison E, Abualrous ET, Kuroпка B, Freund C (2018) Quantification of HLA-DM-dependent major histocompatibility complex of class II immunopeptidomes by the peptide landscape antigenic epitope alignment utility. *Front Immunol* 9: 872
- Anderson KS, Cresswell P (1994) A role for calnexin (IP90) in the assembly of class II MHC molecules. *EMBO J* 13: 675–682
- Arunachalam B, Cresswell P (1995) Molecular requirements for the interaction of class II major histocompatibility complex molecules and invariant chain with calnexin. *J Biol Chem* 270: 2784–2790
- Bakke O, Dobberstein B (1990) MHC class II-associated invariant chain contains a sorting signal for endosomal compartments. *Cell* 63: 707–716
- Bania J, Gatti E, Lelouard H, David A, Cappello F, Weber E, Camosseto V, Pierre P (2003) Human cathepsin S, but not cathepsin L, degrades efficiently MHC class II-associated invariant chain in nonprofessional APCs. *Proc Natl Acad Sci U S A* 100: 6664–6669
- Benaroch P, Yilla M, Raposo G, Ito K, Miwa K, Geuze HJ, Ploegh HL (1995) How MHC class II molecules reach the endocytic pathway. *EMBO J* 14: 37–49
- Bijlmakers MJ, Benaroch P, Ploegh HL (1994) Assembly of HLA DR1 molecules translated in vitro: binding of peptide in the endoplasmic reticulum precludes association with invariant chain. *EMBO J* 13: 2699–2707
- Bikoff E, Birshtein BK (1986) T cell clones specific for IgG2a of the a allotype: direct evidence for presentation of endogenous antigen. *J Immunol* 137: 28–34
- Blanchet FP, Moris A, Nikolic DS, Lehmann M, Cardinaud S, Stalder R, Garcia E, Dinkins C, Leuba F, Wu L *et al* (2010) Human immunodeficiency virus-1 inhibition of immunoamphisomes in dendritic cells impairs early innate and adaptive immune responses. *Immunity* 32: 654–669
- Bruchez A, Sha K, Johnson J, Chen L, Stefani C, McConnell H, Gaucherand L, Prins R, Matreyek KA, Hume AJ *et al* (2020) MHC class II transactivator CIITA induces cell resistance to Ebola virus and SARS-like coronaviruses. *Science* 370: 241–247
- Busch R, Cloutier I, Sekaly RP, Hammerling GJ (1996) Invariant chain protects class II histocompatibility antigens from binding intact polypeptides in the endoplasmic reticulum. *EMBO J* 15: 418–428
- Choi H, Larsen B, Lin ZY, Breitreutz A, Mellacheruvu D, Fermin D, Qin ZS, Tyers M, Gingras AC, Nesvizhskii AI (2011) SAINT: probabilistic scoring of affinity purification-mass spectrometry data. *Nat Methods* 8: 70–73
- Coulon PG, Richetta C, Rouers A, Blanchet FP, Urrutia A, Guerbois M, Piguet V, Theodorou I, Bet A, Schwartz O *et al* (2016) HIV-infected dendritic cells present endogenous MHC class II-restricted antigens to HIV-specific CD4⁺ T cells. *J Immunol* 197: 517–532
- Crotzer VL, Blum JS (2008) Cytosol to lysosome transport of intracellular antigens during immune surveillance. *Traffic* 9: 10–16
- Dani A, Chaudhry A, Mukherjee P, Rajagopal D, Bhatia S, George A, Bal V, Rath S, Mayor S (2004) The pathway for MHCII-mediated presentation of endogenous proteins involves peptide transport to the endo-lysosomal compartment. *J Cell Sci* 117: 4219–4230
- De Angelis Rigotti F, De Gassart A, Pforr C, Cano F, N'Guessan P, Combes A, Camosseto V, Lehner PJ, Pierre P, Gatti E (2017) MARCH9-mediated ubiquitination regulates MHC I export from the TGN. *Immunol Cell Biol* 95: 753–764
- De Gassart A, Camosseto V, Thibodeau J, Ceppi M, Catalan N, Pierre P, Gatti E (2008) MHC class II stabilization at the surface of human dendritic cells is the result of maturation-dependent MARCH I down-regulation. *Proc Natl Acad Sci U S A* 105: 3491–3496
- Dengjel J, Schoor O, Fischer R, Reich M, Kraus M, Muller M, Kreymborg K, Altenberend F, Brandenburg J, Kalbacher H *et al* (2005) Autophagy promotes MHC class II presentation of peptides from intracellular source proteins. *Proc Natl Acad Sci U S A* 102: 7922–7927
- Denzin LK, Cresswell P (1995) HLA-DM induces CLIP dissociation from MHC class II alpha beta dimers and facilitates peptide loading. *Cell* 82: 155–165
- Diedrich G, Bangia N, Pan M, Cresswell P (2001) A role for calnexin in the assembly of the MHC class I loading complex in the endoplasmic reticulum. *J Immunol* 166: 1703–1709
- Dorfel D, Appel S, Grunebach F, Weck MM, Muller MR, Heine A, Brossart P (2005) Processing and presentation of HLA class I and II epitopes by dendritic cells after transfection with in vitro-transcribed MUC1 RNA. *Blood* 105: 3199–3205

- Eisenlohr LC, Hackett CJ (1989) Class II major histocompatibility complex-restricted T cells specific for a virion structural protein that do not recognize exogenous influenza virus. Evidence that presentation of labile T cell determinants is favored by endogenous antigen synthesis. *J Exp Med* 169: 921–931
- Falk K, Rotzschke O, Stevanovic S, Jung G, Rammensee HG (1991) Allele-specific motifs revealed by sequencing of self-peptides eluted from MHC molecules. *Nature* 351: 290–296
- Fletcher K, Ulferts R, Jacquin E, Veith T, Gammoh N, Arasteh JM, Mayer U, Carding SR, Wileman T, Beale R et al (2018) The WD40 domain of ATG16L1 is required for its non-canonical role in lipidation of LC3 at single membranes. *EMBO J* 37: e97840
- Fonteneau JF, Brilot F, Munz C, Gannage M (2016) The tumor antigen NY-ESO-1 mediates direct recognition of melanoma cells by CD4⁺ T cells after intercellular antigen transfer. *J Immunol* 196: 64–71
- Forgac M (2007) Vacuolar ATPases: rotary proton pumps in physiology and pathophysiology. *Nat Rev Mol Cell Biol* 8: 917–929
- Fu T, Liu J, Wang Y, Xie X, Hu S, Pan L (2018) Mechanistic insights into the interactions of NAP1 with the SKICH domains of NDP52 and TAX1BP1. *Proc Natl Acad Sci U S A* 115: e11651–e11660
- Germain RN, Hendrix LR (1991) MHC class II structure, occupancy and surface expression determined by post-endoplasmic reticulum antigen binding. *Nature* 353: 134–139
- Ghosh M, Di Marco M, Stevanovic S (2019) Identification of MHC ligands and establishing MHC class I peptide motifs. *Methods Mol Biol* 1988: 137–147
- Hayer A, Shao L, Chung M, Joubert LM, Yang HW, Tsai FC, Bisaria A, Betzig E, Meyer T (2016) Engulfed cadherin fingers are polarized junctional structures between collectively migrating endothelial cells. *Nat Cell Biol* 18: 1311–1323
- Hu S, Wang Y, Gong Y, Liu J, Li Y, Pan L (2018) Mechanistic insights into recognitions of ubiquitin and myosin VI by autophagy receptor TAX1BP1. *J Mol Biol* 430: 3283–3296
- Jacobson S, Sekaly RP, Bellini WJ, Johnson CL, McFarland HF, Long EO (1988) Recognition of intracellular measles virus antigens by HLA class II restricted measles virus-specific cytotoxic T lymphocytes. *Ann N Y Acad Sci* 540: 352–353
- Jagannath C, Lindsey DR, Dhandayuthapani S, Xu Y, Hunter RL Jr, Eissa NT (2009) Autophagy enhances the efficacy of BCG vaccine by increasing peptide presentation in mouse dendritic cells. *Nat Med* 15: 267–276
- Jaraquemada D, Marti M, Long EO (1990) An endogenous processing pathway in vaccinia virus-infected cells for presentation of cytoplasmic antigens to class II-restricted T cells. *J Exp Med* 172: 947–954
- Jin Y, Sun C, Feng L, Li P, Xiao L, Ren Y, Wang D, Li C, Chen L (2014) Regulation of SIV antigen-specific CD4⁺ T cellular immunity via autophagosome-mediated MHC II molecule-targeting antigen presentation in mice. *PLoS One* 9: e93143
- Johnson DE, Ostrowski P, Jaumouillé V, Grinstein S (2016) The position of lysosomes within the cell determines their luminal pH. *J Cell Biol* 212: 677–692
- Jongsma ML, Berlin I, Wijdeven RH, Janssen L, Janssen GM, Garstka MA, Janssen H, Mensink M, van Veelen PA, Spaapen RM et al (2016) An ER-associated pathway defines endosomal architecture for controlled cargo transport. *Cell* 166: 152–166
- Jurtz V, Paul S, Andreatta M, Marcatili P, Peters B, Nielsen M (2017) NetMHCpan-4.0: improved peptide-MHC class I interaction predictions integrating eluted ligand and peptide binding affinity data. *J Immunol* 199: 3360–3368
- Käll L, Canterbury JD, Weston J, Noble WS, MacCoss MJ (2007) Semi-supervised learning for peptide identification from shotgun proteomics datasets. *Nat Methods* 4: 923–925
- Kirkin V (2020) History of the selective autophagy research: how did it begin and where does it stand today? *J Mol Biol* 432: 3–27
- Kirkin V, Rogov VV (2019) A diversity of selective autophagy receptors determines the specificity of the autophagy pathway. *Mol Cell* 76: 268–285
- Lakkaraju AK, Abrami L, Lemmin T, Blaskovic S, Kunz B, Kihara A, Dal Peraro M, van der Goot FG (2012) Palmitoylated calnexin is a key component of the ribosome-translocon complex. *EMBO J* 31: 1823–1835
- Lapaque N, Jahnke M, Trowsdale J, Kelly AP (2009) The HLA-DR α chain is modified by polyubiquitination. *J Biol Chem* 284: 7007–7016
- Lee HK, Mattei LM, Steinberg BE, Alberts P, Lee YH, Chervonsky A, Mizushima N, Grinstein S, Iwasaki A (2010) *In vivo* requirement for Atg5 in antigen presentation by dendritic cells. *Immunity* 32: 227–239
- Leung CS (2015) Endogenous antigen presentation of MHC class II epitopes through non-autophagic pathways. *Front Immunol* 6: 464
- Lich JD, Elliott JF, Blum JS (2000) Cytoplasmic processing is a prerequisite for presentation of an endogenous antigen by major histocompatibility complex class II proteins. *J Exp Med* 191: 1513–1524
- Lin CY, Nozawa T, Minowa-Nozawa A, Toh H, Aikawa C, Nakagawa I (2019) LAMTOR2/LAMTOR1 complex is required for TAX1BP1-mediated xenophagy. *Cell Microbiol* 21: e12981
- Lotteau V, Teyton L, Peleraux A, Nilsson T, Karlsson L, Schmid SL, Quaranta V, Peterson PA (1990) Intracellular transport of class II MHC molecules directed by invariant chain. *Nature* 348: 600–605
- Lynes EM, Raturi A, Shenkman M, Ortiz Sandoval C, Yap MC, Wu J, Janowicz A, Myhill N, Benson MD, Campbell RE et al (2013) Palmitoylation is the switch that assigns calnexin to quality control or ER Ca²⁺ signaling. *J Cell Sci* 126: 3893–3903
- Malnati MS, Marti M, LaVaute T, Jaraquemada D, Biddison W, DeMars R, Long EO (1992) Processing pathways for presentation of cytosolic antigen to MHC class II-restricted T cells. *Nature* 357: 702–704
- Manoury B, Mazzeo D, Li DN, Billson J, Loak K, Benaroch P, Watts C (2003) Asparagine endopeptidase can initiate the removal of the MHC class II invariant chain chaperone. *Immunity* 18: 489–498
- Marcu A, Bichmann L, Kuchenbecker L, Kowalewski DJ, Freudenmann LK, Backert L, Mühlenthaler L, Szolek A, Lübke M, Wagner P et al (2021) HLA Ligand Atlas: a benign reference of HLA-presented peptides to improve T-cell-based cancer immunotherapy. *J Immunother Cancer* 9: e002071
- Margiotta A, Frei DM, Sendstad IH, Janssen L, Neefjes J, Bakke O (2020) Invariant chain regulates endosomal fusion and maturation through an interaction with the SNARE Vti1b. *J Cell Sci* 133: jcs244624
- Mellacheruvu D, Wright Z, Couzens AL, Lambert JP, St-Denis NA, Li T, Miteva YV, Hauri S, Sardiou ME, Low TY et al (2013) The CRAPome: a contaminant repository for affinity purification-mass spectrometry data. *Nat Methods* 10: 730–736
- Mildenberger J, Johansson I, Sergin I, Kjobli E, Damas JK, Razani B, Flo TH, Bjorkoy G (2017) N-3 PUFAs induce inflammatory tolerance by formation of KEAP1-containing SQSTM1/p62-bodies and activation of NFE2L2. *Autophagy* 13: 1664–1678
- Miller MA, Ganesan AP, Luckashenak N, Mendonca M, Eisenlohr LC (2015) Endogenous antigen processing drives the primary CD4⁺ T cell response to influenza. *Nat Med* 21: 1216–1222
- Moris A, Pajot A, Blanchet F, Guivel-Benhassine F, Salcedo M, Schwartz O (2006) Dendritic cells and HIV-specific CD4⁺ T cells: HIV antigen presentation, T-cell activation, and viral transfer. *Blood* 108: 1643–1651

- Morris P, Shaman J, Attaya M, Amaya M, Goodman S, Bergman C, Monaco JJ, Mellins E (1994) An essential role for HLA-DM in antigen presentation by class II major histocompatibility molecules. *Nature* 368: 551–554
- Morriswood B, Ryzhakov G, Puri C, Arden SD, Roberts R, Dendrou C, Kendrick-Jones J, Buss F (2007) T6BP and NDP52 are myosin VI binding partners with potential roles in cytokine signalling and cell adhesion. *J Cell Sci* 120: 2574–2585
- Mukherjee P, Dani A, Bhatia S, Singh N, Rudensky AY, George A, Bal V, Mayor S, Rath S (2001) Efficient presentation of both cytosolic and endogenous transmembrane protein antigens on MHC class II is dependent on cytoplasmic proteolysis. *J Immunol* 167: 2632–2641
- Muntasell A, Carrascal M, Alvarez I, Serradell L, van Veelen P, Verreck FA, Koning F, Abian J, Jaraquemada D (2004) Dissection of the HLA-DR4 peptide repertoire in endocrine epithelial cells: strong influence of invariant chain and HLA-DM expression on the nature of ligands. *J Immunol* 173: 1085–1093
- Muntasell A, Carrascal M, Serradell L, Veelen P, Verreck F, Koning F, Raposo G, Abián J, Jaraquemada D (2002) HLA-DR4 molecules in neuroendocrine epithelial cells associate to a heterogeneous repertoire of cytoplasmic and surface self peptides. *J Immunol* 169: 5052–5060
- Myhill N, Lynes EM, Nanji JA, Blagoveshchenskaya AD, Fei H, Carmine Simmen K, Cooper TJ, Thomas G, Simmen T (2008) The subcellular distribution of calnexin is mediated by PACS-2. *Mol Biol Cell* 19: 2777–2788
- Nakagawa T, Roth W, Wong P, Nelson A, Farr A, Deussing J, Villadangos JA, Ploegh H, Peters C, Rudensky AY (1998) Cathepsin L: critical role in li degradation and CD4 T cell selection in the thymus. *Science* 280: 450–453
- Neeffes J, Jongsma MML, Berlin I (2017) Stop or Go? Endosome positioning in the establishment of compartment architecture, dynamics, and function. *Trends Cell Biol* 27: 580–594
- Neeffes JJ, Stollorz V, Peters PJ, Geuze HJ, Ploegh HL (1990) The biosynthetic pathway of MHC class II but not class I molecules intersects the endocytic route. *Cell* 61: 171–183
- Nelde A, Kowalewski DJ, Stevanovic S (2019) Purification and identification of naturally presented MHC class I and II ligands. *Methods Mol Biol* 1988: 123–136
- Nuchtern JG, Biddison WE, Klausner RD (1990) Class II MHC molecules can use the endogenous pathway of antigen presentation. *Nature* 343: 74–76
- O'Loughlin T, Masters TA, Buss F (2018) The MYO6 interactome reveals adaptor complexes coordinating early endosome and cytoskeletal dynamics. *EMBO Rep* 19: e44884
- Paludan C, Schmid D, Landthaler M, Vockerodt M, Kube D, Tuschl T, Munz C (2005) Endogenous MHC class II processing of a viral nuclear antigen after autophagy. *Science* 307: 593–596
- Pathan M, Keerthikumar S, Ang CS, Gangoda L, Quek CY, Williamson NA, Mouradov D, Sieber OM, Simpson RJ, Salim A et al (2015) FunRich: An open access standalone functional enrichment and interaction network analysis tool. *Proteomics* 15: 2597–2601
- Perez-Riverol Y, Csordas A, Bai J, Bernal-Llinares M, Hewapathirana S, Kundu DJ, Inuganti A, Griss J, Mayer G, Eisenacher M et al (2019) The PRIDE database and related tools and resources in 2019: improving support for quantification data. *Nucleic Acids Res* 47: D442–D450
- Petkova DS, Verlhac P, Rozieres A, Baguet J, Claviere M, Kretz-Remy C, Mahieux R, Viret C, Faure M (2017) Distinct contributions of autophagy receptors in measles virus replication. *Viruses* 9: 123
- Pinet V, Vergelli M, Martin R, Bakke O, Long EO (1995) Antigen presentation mediated by recycling of surface HLA-DR molecules. *Nature* 375: 603–606
- Prasad SA, Yewdell JW, Porgador A, Sadasivan B, Cresswell P, Bennink JR (1998) Calnexin expression does not enhance the generation of MHC class I-peptide complexes. *Eur J Immunol* 28: 907–913
- Ramachandra L, Kovats S, Eastman S, Rudensky AY (1996) Variation in HLA-DM expression influences conversion of MHC class II alpha beta: class II-associated invariant chain peptide complexes to mature peptide-bound class II alpha beta dimers in a normal B cell line. *J Immunol* 156: 2196–2204
- Rammensee H, Bachmann J, Emmerich NP, Bachor OA, Stevanovic S (1999) SYFPEITHI: database for MHC ligands and peptide motifs. *Immunogenetics* 50: 213–219
- Randow F, Youle RJ (2014) Self and nonself: how autophagy targets mitochondria and bacteria. *Cell Host Microbe* 15: 403–411
- Reith W, Leibundgut-Landmann S, Waldburger JM (2005) Regulation of MHC class II gene expression by the class II transactivator. *Nat Rev Immunol* 5: 793–806
- Reynisson B, Barra C, Kaabinejadian S, Hildebrand WH, Peters B, Nielsen M (2020) Improved prediction of MHC II antigen presentation through integration and motif deconvolution of mass spectrometry MHC eluted ligand data. *J Proteome Res* 19: 2304–2315
- Richter B, Sliter DA, Herhaus L, Stolz A, Wang C, Beli P, Zaffagnini G, Wild P, Martens S, Wagner SA et al (2016) Phosphorylation of OPTN by TBK1 enhances its binding to Ub chains and promotes selective autophagy of damaged mitochondria. *Proc Natl Acad Sci U S A* 113: 4039–4044
- Riese RJ, Wolf PR, Bromme D, Natkin LR, Villadangos JA, Ploegh HL, Chapman HA (1996) Essential role for cathepsin S in MHC class II-associated invariant chain processing and peptide loading. *Immunity* 4: 357–366
- Roche PA, Cresswell P (1991) Proteolysis of the class II-associated invariant chain generates a peptide binding site in intracellular HLA-DR molecules. *Proc Natl Acad Sci U S A* 88: 3150–3154
- Roche PA, Furuta K (2015) The ins and outs of MHC class II-mediated antigen processing and presentation. *Nat Rev Immunol* 15: 203–216
- Roche PA, Marks MS, Cresswell P (1991) Formation of a nine-subunit complex by HLA class II glycoproteins and the invariant chain. *Nature* 354: 392–394
- Romagnoli P, Germain RN (1995) Inhibition of invariant chain (II)-calnexin interaction results in enhanced degradation of li but does not prevent the assembly of alpha beta II complexes. *J Exp Med* 182: 2027–2036
- Romagnoli P, Layet C, Yewdell J, Bakke O, Germain RN (1993) Relationship between invariant chain expression and major histocompatibility complex class II transport into early and late endocytic compartments. *J Exp Med* 177: 583–596
- Rudensky A, Preston-Hurlburt P, Hong SC, Barlow A, Janeway CA Jr (1991) Sequence analysis of peptides bound to MHC class II molecules. *Nature* 353: 622–627
- Rudensky AY, Yurin VL (1989) Immunoglobulin-specific T-B cell interaction. I. Presentation of self immunoglobulin determinants by B lymphocytes. *Eur J Immunol* 19: 1677–1683
- Sahlender DA, Roberts RC, Arden SD, Spudich G, Taylor MJ, Luzio JP, Kendrick-Jones J, Buss F (2005) Optineurin links myosin VI to the Golgi complex and is involved in Golgi organization and exocytosis. *J Cell Biol* 169: 285–295
- Sanderson F, Kleijmeer MJ, Kelly A, Verwoerd D, Tulp A, Neeffes JJ, Geuze HJ, Trowsdale J (1994) Accumulation of HLA-DM, a regulator of antigen presentation, in MHC class II compartments. *Science* 266: 1566–1569
- Schmid D, Pypaert M, Munz C (2007) Antigen-loading compartments for major histocompatibility complex class II molecules continuously receive input from autophagosomes. *Immunity* 26: 79–92

- Schröder B (2016) The multifaceted roles of the invariant chain CD74—more than just a chaperone. *Biochim Biophys Acta* 1863: 1269–1281
- Schuster C, Gerold KD, Schober K, Probst L, Boerner K, Kim MJ, Ruckdeschel A, Serwold T, Kissler S (2015) The autoimmunity-associated gene CLEC16A modulates thymic epithelial cell autophagy and alters T cell selection. *Immunity* 42: 942–952
- Scott JE, Dawson JR (1995) MHC class I expression and transport in a calnexin-deficient cell line. *J Immunol* 155: 143–148
- Sekaly RP, Jacobson S, Richert JR, Tonnelle C, McFarland HF, Long EO (1988) Antigen presentation to HLA class II-restricted measles virus-specific T-cell clones can occur in the absence of the invariant chain. *Proc Natl Acad Sci U S A* 85: 1209–1212
- Shembade N, Harhaj NS, Parvatiyar K, Copeland NG, Jenkins NA, Matesic LE, Harhaj EW (2008) The E3 ligase Itch negatively regulates inflammatory signaling pathways by controlling the function of the ubiquitin-editing enzyme A20. *Nat Immunol* 9: 254–262
- Shembade N, Ma A, Harhaj EW (2010) Inhibition of NF-kappaB signaling by A20 through disruption of ubiquitin enzyme complexes. *Science* 327: 1135–1139
- Shi GP, Bryant RA, Riese R, Verhelst S, Driessen C, Li Z, Bromme D, Ploegh HL, Chapman HA (2000) Role for cathepsin F in invariant chain processing and major histocompatibility complex class II peptide loading by macrophages. *J Exp Med* 191: 1177–1186
- Shin JS, Ebersold M, Pypaert M, Delamarre L, Hartley A, Mellman I (2006) Surface expression of MHC class II in dendritic cells is controlled by regulated ubiquitination. *Nature* 444: 115–118
- Sinnathamby G, Eisenlohr LC (2003) Presentation by recycling MHC class II molecules of an influenza hemagglutinin-derived epitope that is revealed in the early endosome by acidification. *J Immunol* 170: 3504–3513
- Tewari MK, Sinnathamby G, Rajagopal D, Eisenlohr LC (2005) A cytosolic pathway for MHC class II-restricted antigen processing that is proteasome and TAP dependent. *Nat Immunol* 6: 287–294
- Thibodeau J, Moulefera MA, Balthazard R (2019) On the structure-function of MHC class II molecules and how single amino acid polymorphisms could alter intracellular trafficking. *Hum Immunol* 80: 15–31
- Thiele F, Tao S, Zhang Y, Muschaweckh A, Zollmann T, Protzer U, Abele R, Drexler I (2015) Modified vaccinia virus Ankara-infected dendritic cells present CD4⁺ T-cell epitopes by endogenous major histocompatibility complex class II presentation pathways. *J Virol* 89: 2698–2709
- Thurston TL, Ryzhakov G, Bloor S, von Muhlinen N, Randow F (2009) The TBK1 adaptor and autophagy receptor NDP52 restricts the proliferation of ubiquitin-coated bacteria. *Nat Immunol* 10: 1215–1221
- Tsuji T, Matsuzaki J, Caballero OL, Jungbluth AA, Ritter G, Odunsi K, Old LJ, Gnjjatic S (2012) Heat shock protein 90-mediated peptide-selective presentation of cytosolic tumor antigen for direct recognition of tumors by CD4(+) T cells. *J Immunol* 188: 3851–3858
- Tumbarello DA, Manna PT, Allen M, Bycroft M, Arden SD, Kendrick-Jones J, Buss F (2015) The autophagy receptor TAX1BP1 and the molecular motor myosin VI are required for clearance of salmonella typhimurium by autophagy. *PLoS Pathog* 11: e1005174
- Tumbarello DA, Waxse BJ, Arden SD, Bright NA, Kendrick-Jones J, Buss F (2012) Autophagy receptors link myosin VI to autophagosomes to mediate Tom1-dependent autophagosome maturation and fusion with the lysosome. *Nat Cell Biol* 14: 1024–1035
- Tyanova S, Temu T, Sinitcyn P, Carlson A, Hein MY, Geiger T, Mann M, Cox J (2016) The Perseus computational platform for comprehensive analysis of (prote)omics data. *Nat Methods* 13: 731–740
- Unanue ER, Turk V, Neeffjes J (2016) Variations in MHC class II antigen processing and presentation in health and disease. *Annu Rev Immunol* 34: 265–297
- Vassilakos A, Cohen-Doyle MF, Peterson PA, Jackson MR, Williams DB (1996) The molecular chaperone calnexin facilitates folding and assembly of class I histocompatibility molecules. *EMBO J* 15: 1495–1506
- Veerappan Ganesan AP, Eisenlohr LC (2017) The elucidation of non-classical MHC class II antigen processing through the study of viral antigens. *Curr Opin Virol* 22: 71–76
- Verlhac P, Gregoire IP, Azocar O, Petkova DS, Baguet J, Viret C, Faure M (2015) Autophagy receptor NDP52 regulates pathogen-containing autophagosome maturation. *Cell Host Microbe* 17: 515–525
- Walseng E, Furuta K, Bosch B, Weih KA, Matsuki Y, Bakke O, Ishido S, Roche PA (2010) Ubiquitination regulates MHC class II-peptide complex retention and degradation in dendritic cells. *Proc Natl Acad Sci U S A* 107: 20465–20470
- Watts C (2004) The exogenous pathway for antigen presentation on major histocompatibility complex class II and CD1 molecules. *Nat Immunol* 5: 685–692
- Weil R, Laplantine E, Curic S, Génin P (2018) Role of optineurin in the mitochondrial dysfunction: potential implications in neurodegenerative diseases and cancer. *Front Immunol* 9: 1243
- Weiss S, Bogen B (1989) B-lymphoma cells process and present their endogenous immunoglobulin to major histocompatibility complex-restricted T cells. *Proc Natl Acad Sci U S A* 86: 282–286
- Wijdeven RH, van Luijn MM, Wierenga-Wolf AF, Akkermans JJ, van den Elsen PJ, Hintzen RQ, Neeffjes J (2018) Chemical and genetic control of IFN-gamma-induced MHCII expression. *EMBO Rep* 19: e45553
- Wild P, Farhan H, McEwan DG, Wagner S, Rogov VV, Brady NR, Richter B, Korac J, Waidmann O, Choudhary C et al (2011) Phosphorylation of the autophagy receptor optineurin restricts Salmonella growth. *Science* 333: 228–233
- Zhou D, Li P, Lin Y, Lott JM, Hislop AD, Canaday DH, Brutekiewicz RR, Blum JS (2005) Lamp-2a facilitates MHC class II presentation of cytoplasmic antigens. *Immunity* 22: 571–581



License: This is an open access article under the terms of the [Creative Commons Attribution](https://creativecommons.org/licenses/by/4.0/) License, which permits use, distribution and reproduction in any medium, provided the original work is properly cited.

Expanded View Figures

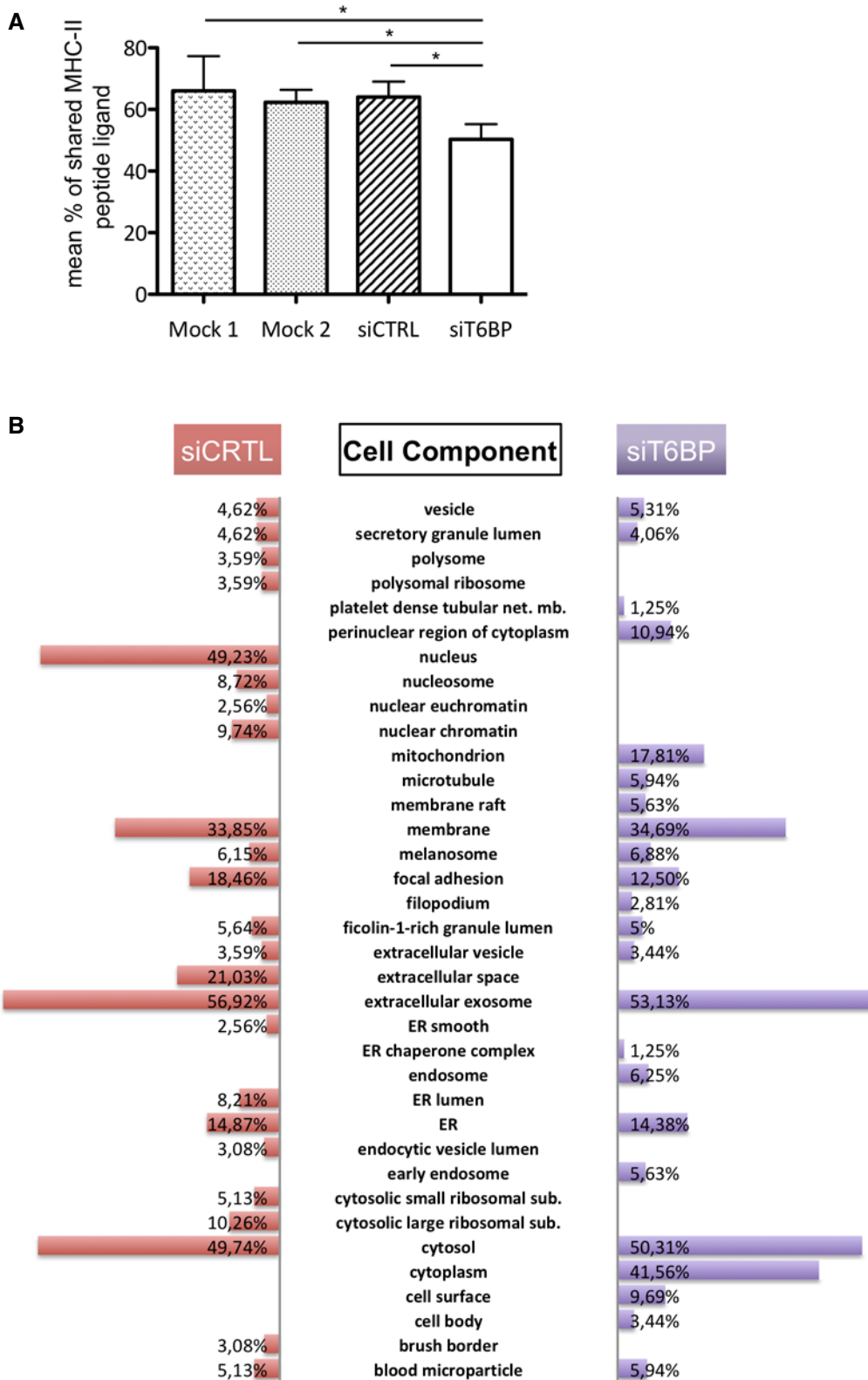


Figure EV1.

Figure EV1. (Related to Fig 3): T6BP silencing affects the repertoire of peptides presented by MHC-II molecules and has a modest influence on the source of MHC-II ligands.

A For each sample the % of MHC-II peptide ligand shared with the 3 other experimental conditions was determined and the mean % of shared MHC-II peptide ligand calculated and plotted (\pm SD). Comparing the mean % of shared peptides between mock treat cells (Mock1 or Mock2) and the cells transfected with the control (siCTRL) siRNA, no significant differences were observed. By contrast, the mean % of shared MHC-II peptide ligand was significantly different between siT6BP-treated cells and Mock1-, Mock2-, and siCTRL-treated cells. The statistical significance was calculated using a Kruskal–Wallis test followed by a Dunn’s test ($*P < 0.05$).

B Cell component enrichment analysis of peptide sources. As in Fig 3, HeLa-CIITA cells were transfected with siCTRL and siT6BP siRNA, lysed, submitted to MHC-II immunoprecipitation using TÛ39 antibody, and the peptide ligands sequenced using mass spectrometry (LC–MS/MS). The diversity of protein sources was analyzed according to cell component enrichment using Funrich software. Only canonical pathways statistically enriched ($P < 0.05$) for each condition (siCTRL and siT6BP) are shown. The P -value for pathway enrichment was obtained using the right-tailed Fisher’s exact test.

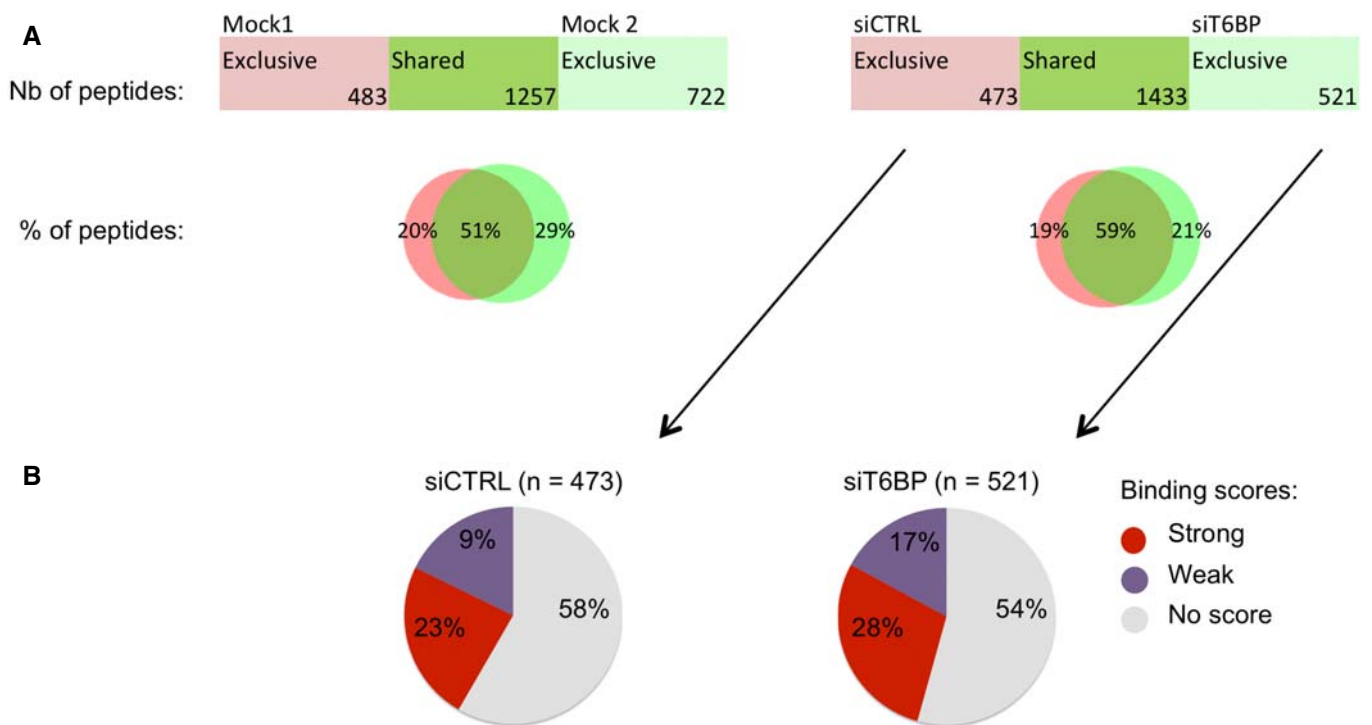


Figure EV2. (Related to Fig 3): T6BP silencing does not influence the immunopeptidome of MHC-I molecules.

A Left panel, mock-treated HeLa-CIITA cells were split and cultured for 48 h (giving rise to Mock1 and Mock2), then cells were lysed, MHC-I molecules were immunoprecipitated using W632 antibody and the peptide ligands sequenced using mass spectrometry (LC–MS/MS). Right panel, HeLa-CIITA cells were transfected with siCTRL and siT6BP siRNA and were treated as in the left panel. The number and the percentage among sequenced peptides (Venn diagrams) of exclusive or shared peptides for each condition are presented.

B Relative binding affinities, presented as pie charts, of exclusive peptides identified in siCTRL (left) and siT6BP (right) condition (number of peptides are indicated in brackets). NetMHCpan 4.0 algorithm was used to predict the relative affinities to HLA-A*6802 and -B*15093 molecules expressed by HeLa-CIITA cells. The relative affinities to the HLA-C*1203 molecule also expressed by HeLa-CIITA cells were not combined in this figure because many peptides binding to HLA-C*1203 also bind to HLA-A*6802. The results are presented as stated from NetMHCpan 4.0 analysis as Strong (for strong binders), Weak (for weak binders), and No score (for epitopes with which a binding score cannot be determined).

Data information: One representative experiment is shown out of two biological replicates. For each experiment, 5 technical replicates per sample were run on the LC–MS/MS. Nb—number; %—percentage.

Figure EV3. (Related to Fig 4). T6BP silencing leads to autophagosome accumulation.

- A LC3 and T6BP expressions were assessed using confocal microscopy. HeLa-ClITA cells were transfected with siCTRL or siT6BP. 48 h post-treatment, LC3 and T6BP were detected using anti-LC3 and anti-T6BP antibodies, respectively. Scale bars: 2 μ m.
- B Quantitative analysis using in-house ImageJ script displaying the number of LC3⁺ vesicles per cell and co-localization using Pearson's coefficient of T6BP and LC3 staining (right panel). 30 cells from two biological replicates were analyzed.
- C, D As in A and B with MHC-II molecule and LC3 staining. A number of cells >40 from two biological replicates were analyzed. Scale bars: 2 μ m.
- E siRNA-treated cells were also analyzed using electron microscopy. Top panels and bottom panels, images from siCTRL- and siT6BP-treated cells, respectively, from 6 representative cells. Two biological replicates were performed and at least 40 cells for each treatment were analyzed. The white arrows indicate the autophagosomes. Scale bars: 1 μ m.
- F As in (A) with HLA-DM and T6BP staining. Scale bars: 4 μ m.
- G The localization of HLA-DM⁺ vesicles and the number of vesicles/cells were quantified as in Fig 4. At least 10,000 vesicles in at least 40 cells were analyzed.

Data information: In graphs representing the number of vesicles/cell, each dot corresponds to a single cell. Within the violin plots, continuous and dotted lines correspond to medians and quartiles, respectively. CTRL: control; nb: number. Mann-Whitney's test; * $P < 0.05$; *** $P < 0.0001$; ns >0.05. For Pearson's coefficient, the dotted lines (at 0.5) indicate the limit under which no significant co-localization is measured.

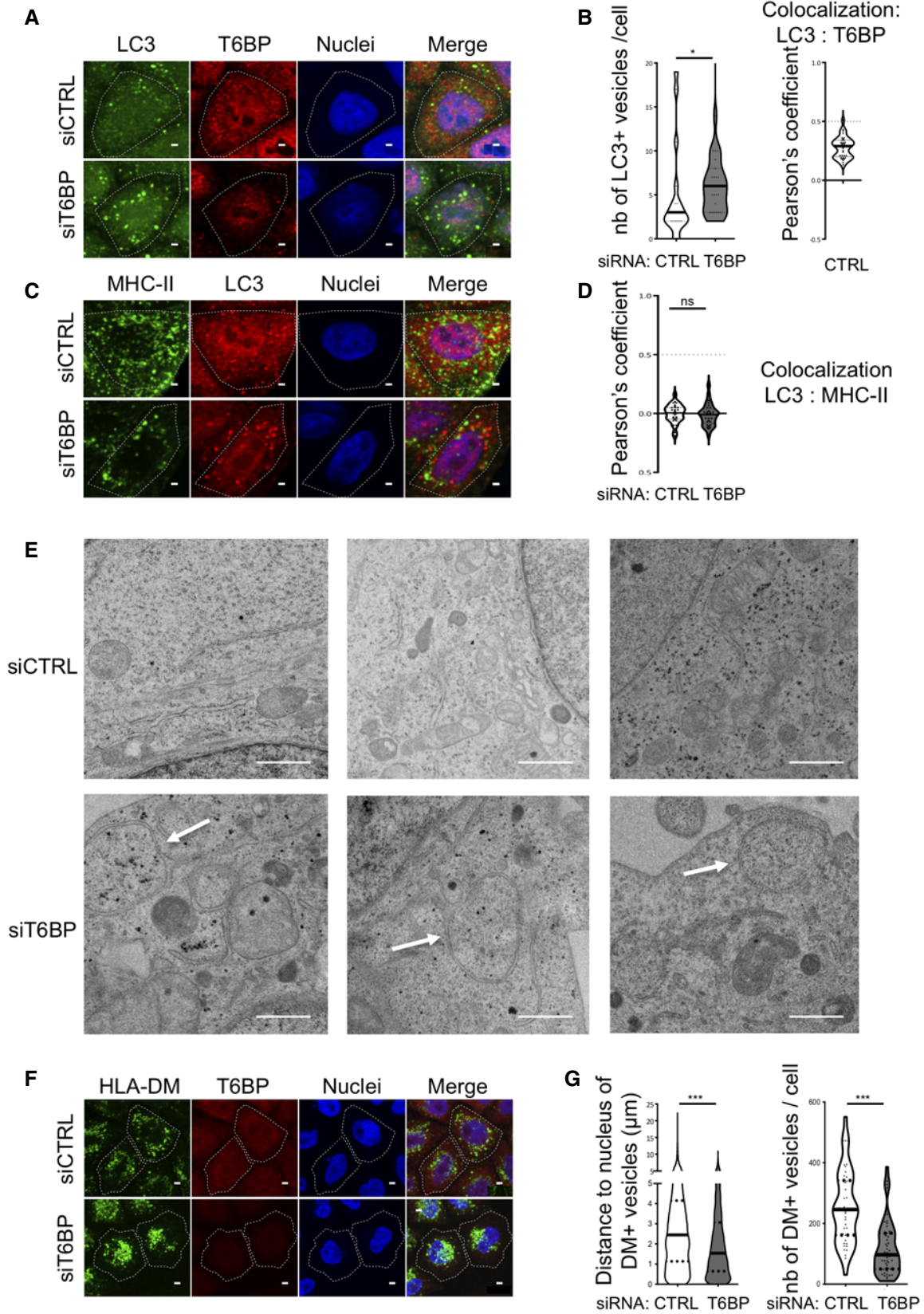


Figure EV3.

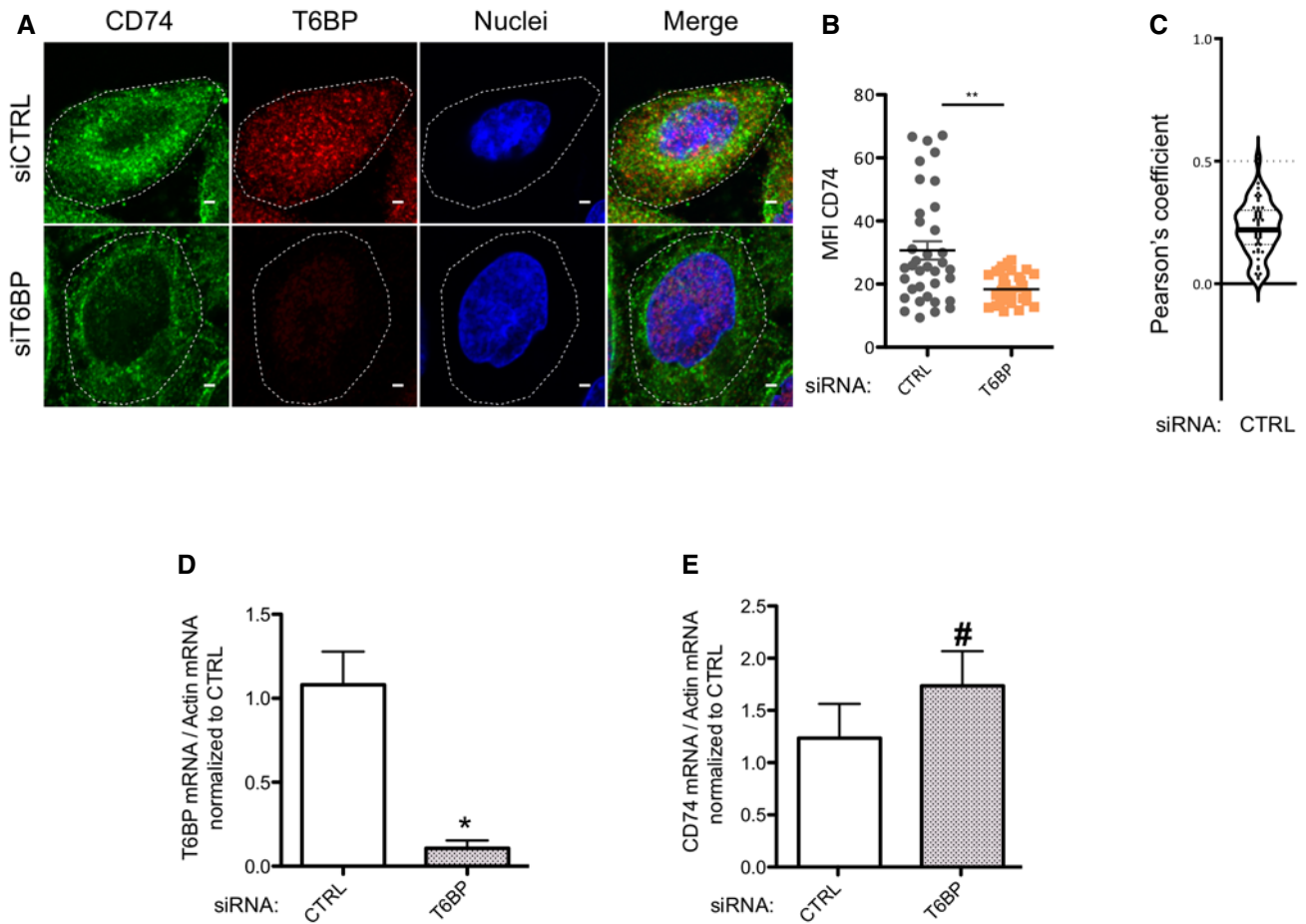


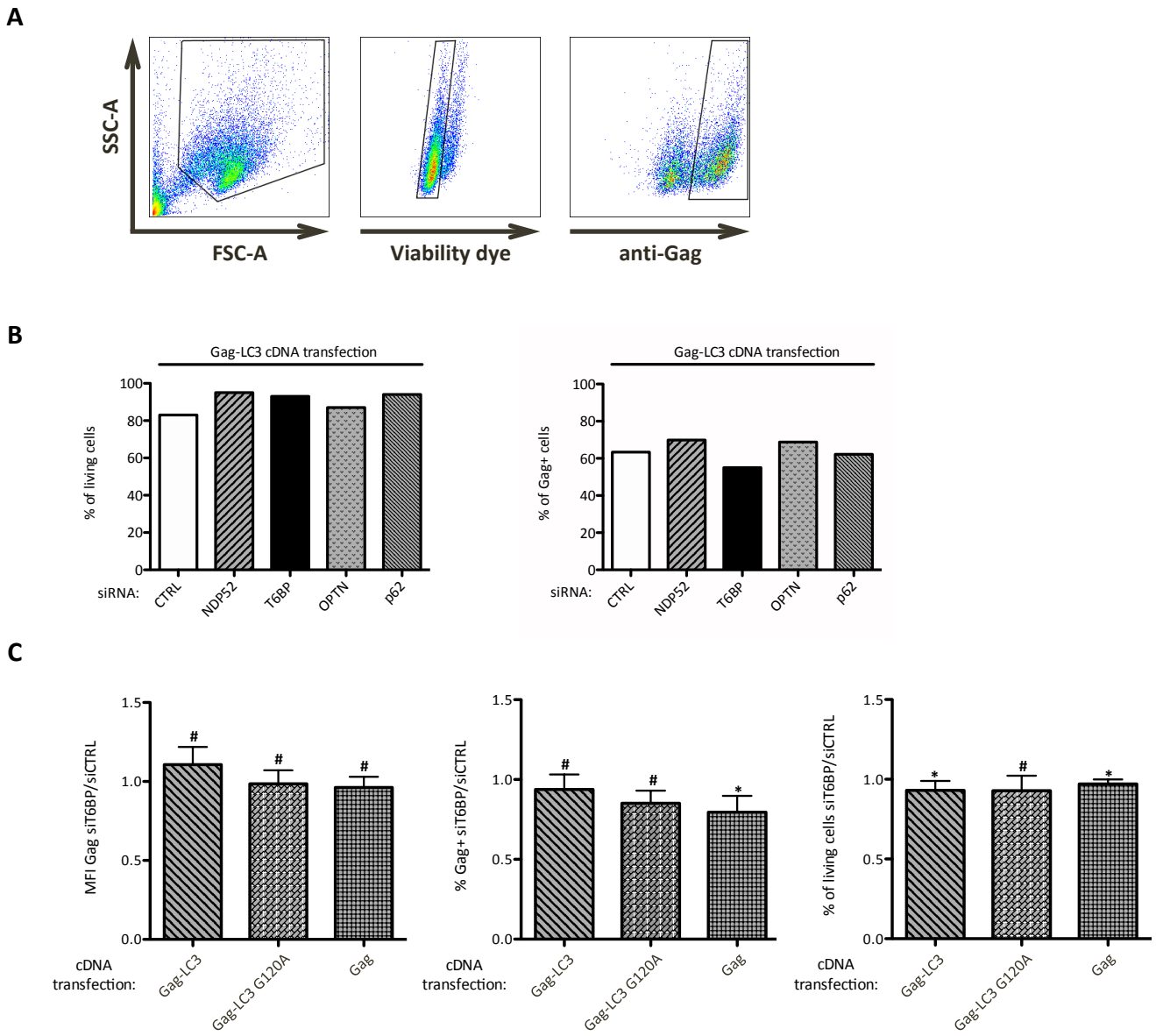
Figure EV4. (Related to Fig 5): T6BP silencing affects CD74 expression levels as assessed by confocal microscopy but does not affect CD74 mRNA levels.

- A CD74 expression assessed using confocal microscopy in HeLa-CIITA cells, 48 h post-treatment with the indicated siRNA. Top panels siCTRL and bottom panels siT6BP. Scale bars: 2 μ m.
- B Quantitative analysis using ImageJ of CD74 mean fluorescent intensity (MFI). The data are representative of at least 3 biological replicates. Each dot displayed corresponds to a single cell. At least 75 cells were analyzed. The continuous lines represent the means (\pm SD). Mann-Whitney's test; ** $P < 0.002$.
- C Co-localization of CD74 and T6BP assessed, in the control condition, using Pearson's coefficient. Number of cells = 47. Within the violin plots, continuous and dotted lines correspond to medians and quartiles, respectively. The dotted lines at 0.5 indicate the limit under which no significant co-localization is measured.
- D, E (D) T6BP and (E) CD74 mRNA levels were assessed using RT-qPCR. HeLa-CIITA cells were transfected with siCTRL and siT6BP. 48 h post-treatment, relative T6BP (D) and CD74 (E) mRNA expression levels were analyzed by RT-qPCR using actin as reference gene. Results are presented as the mean ratios of T6BP (D) and CD74 mRNA (E) levels to actin mRNA levels (\pm SD) from four biological replicates. CTRL—control. Mann-Whitney's test: * $P < 0.05$; # $P > 0.05$.

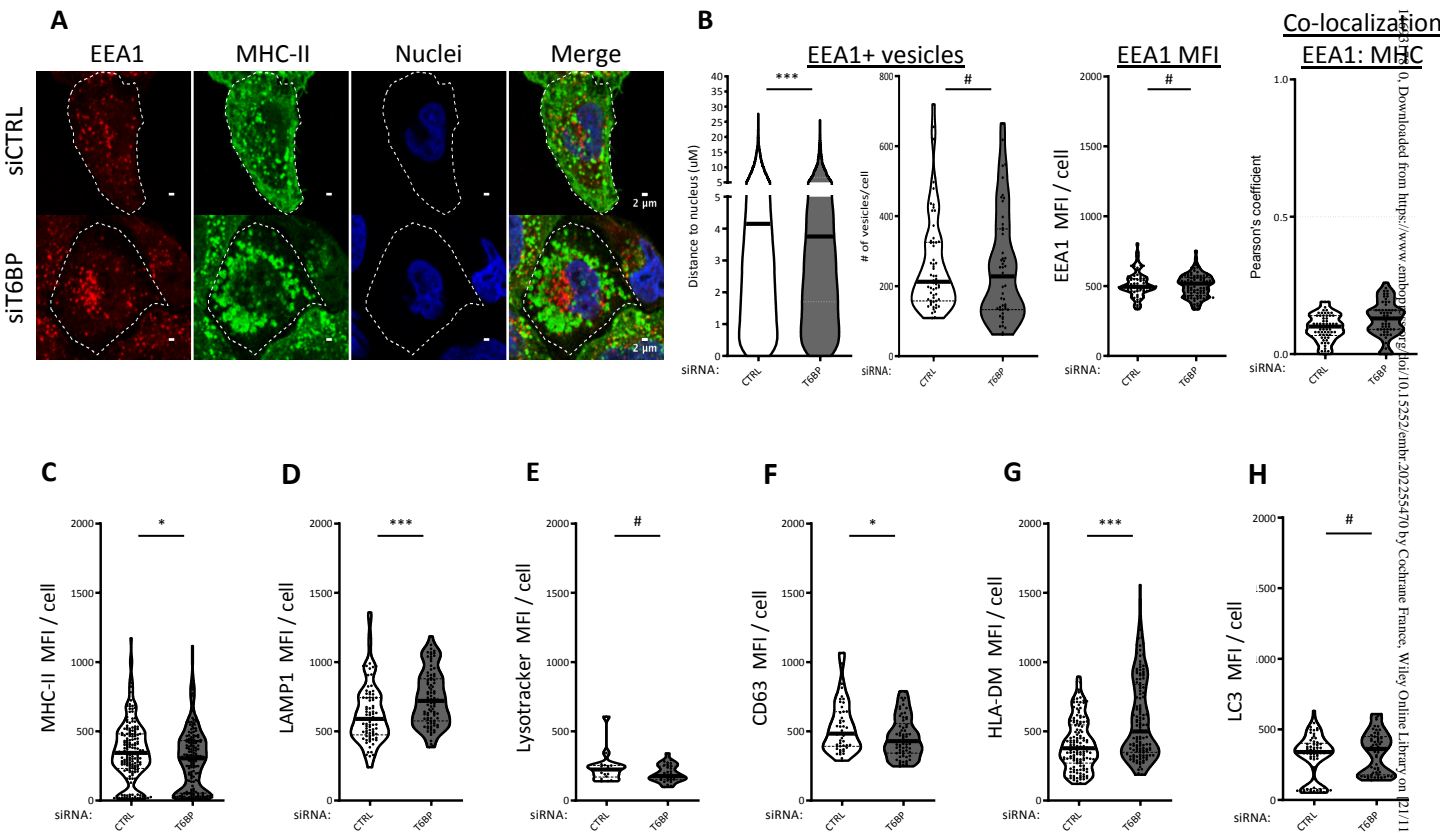
Appendix

Table of content:

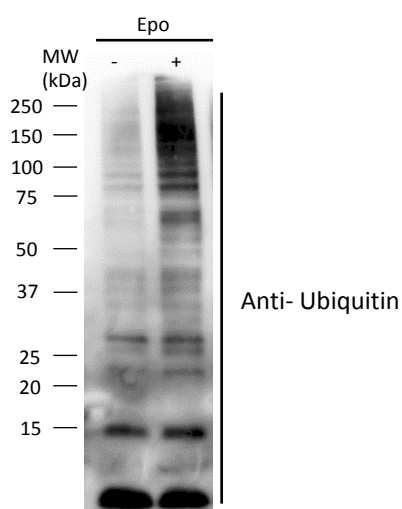
Appendix Figure-S1 (related to Figure-1)	page-2
Appendix Figure-S2 (related to Figure-4)	page-3
Appendix Figure-S3 (related to Figure-5)	page-4
Appendix Figure-S4 (related to Figure-6)	page-5
Appendix Table S1 (related to EV4)	page-6



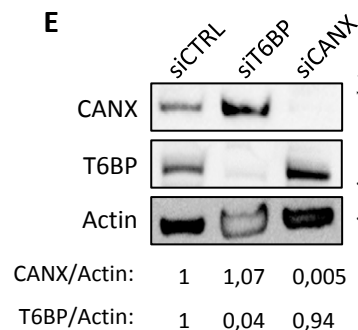
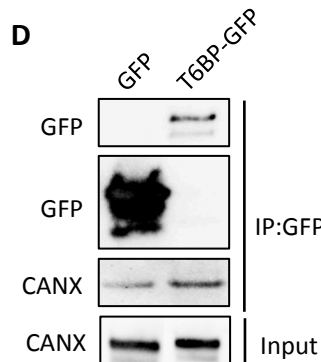
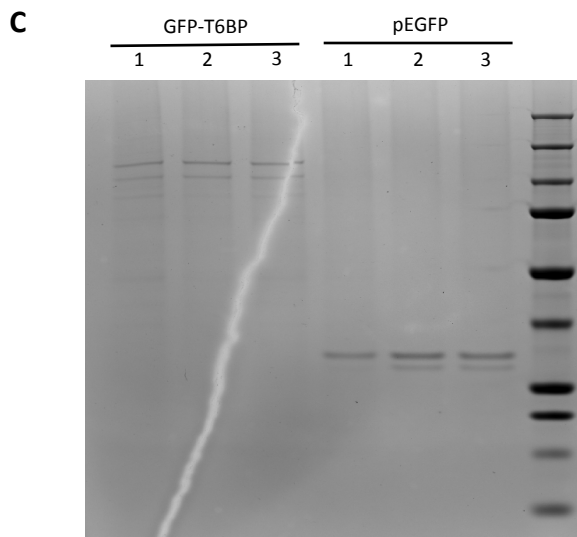
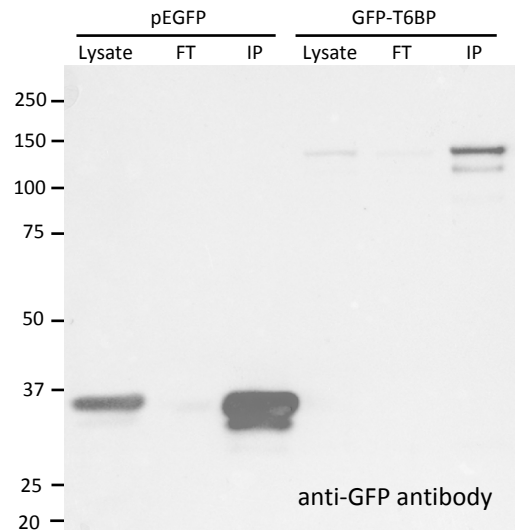
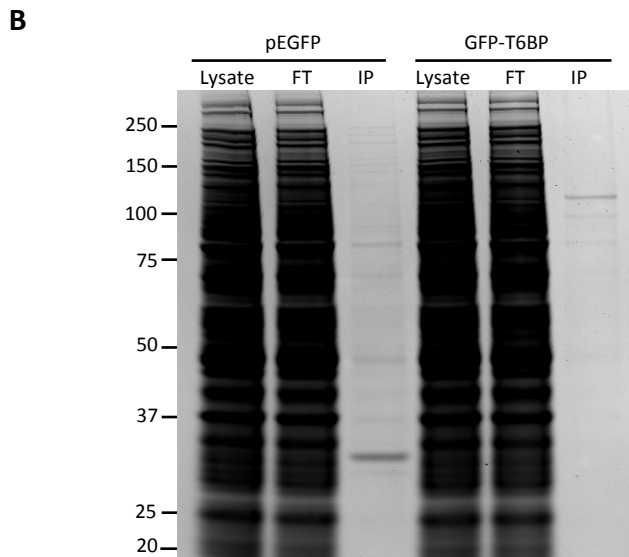
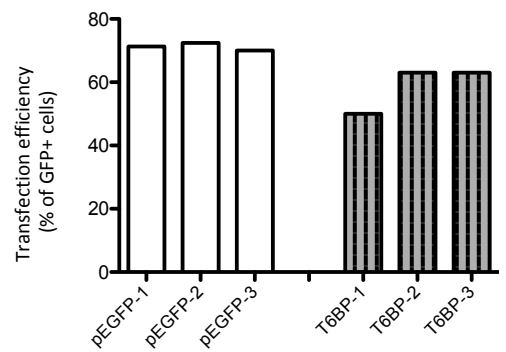
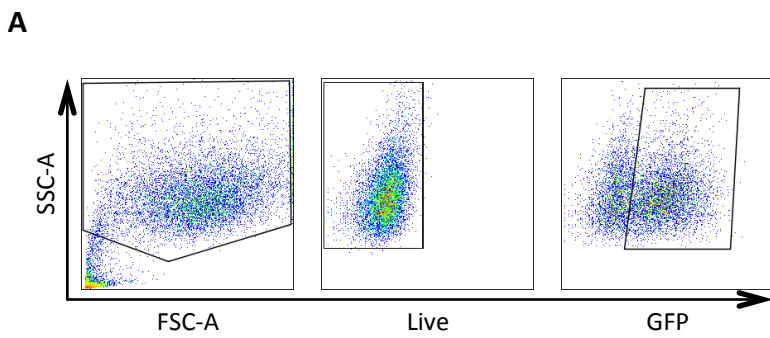
Appendix Figure-S1 (related to Figure-1): The transfection of siRNA targeting autophagy receptors influenced neither the cell viability nor the antigen transfection efficiencies. (A) and (B) Analysis of cell viability and transfection efficiency using flow cytometry. Results of one representative experiment out of three are shown. **(A)** Gating strategy: left panel: FSC-A: forward-scatter; SSC-A: side-scatter; middle panel: staining of living cells using a viability dye; right panel: staining of Gag⁺ cells using anti-Gag antibody intracellular staining. **(B)** Percentage of living and Gag⁺ cells in the different siRNA transfection conditions, left and right panel respectively, analyzed 48h post-treatment, prior co-culture with Gag-specific T cells. **(C)** Results of at least three independent experiments are normalized to control conditions and presented as mean (+/- SD). Left panel, ratio of mean fluorescent intensities (MFI) of Gag stainings in Gag⁺ cells. Middle panel, ratio of the mean percentage of Gag⁺ cells. Right panel, ratio of the mean percentage of living cells. CTRL: control. Mann-Whitney's tests; *p<0.05; #p>0.05.



Appendix Figure S2 (related to Figure-4): T6BP silencing slightly influences EEA1+ vesicle cellular localization (A) EEA1 expression was assessed using confocal microscopy. HeLa-CIITA cells were transfected with siCTRL and siT6BP. 48h post-treatment, EEA1 were detected using specific antibody and a fluorescent secondary antibody. Nuclei were stained using DAPI. **(B)** Quantitative analysis using in-house ImageJ script displaying distance of each EEA1+ vesicles to the nucleus, number of EEA1+ vesicles per cell and EEA1 total MFI per cell. At least 16 000 vesicles from 90 cells corresponding to 3 independent experiments were analyzed. **(B, Right panel)** EEA1 and MHC-II stainings do not colocalize. Quantification of the potential colocalization between MHC-II+ and EEA1+ dots using Pearson's coefficient where the dotted lines (at 0.5) indicate the limit under which no significant co-localization is measured. **(C-H) Effect of siT6BP silencing on the expression levels of the various vesicular markers.** As in A, HeLa-CIITA cells were transfected with siCTRL and siT6BP. 48h post-treatment, cells were fixed and labeled and the MFI of the indicated markers were analyzed. **(C)** MHC-II, at least 170 cells corresponding to 5 independent experiments were analyzed. **(D)** LAMP-1, at least 85 cells corresponding to 3 independent experiments were analyzed. **(E)** Lysotracker, at least 30 cells corresponding to 2 independent experiments were analyzed. **(F)** CD63, at least 60 cells corresponding to 2 independent experiments were analyzed. **(G)** HLA-DM, at least 140 cells corresponding to 3 independent experiments were analyzed. **(H)** LC3, at least 60 cells corresponding to 2 independent experiments were analyzed. In graphs representing the number of vesicles or the MFI per cell, each dot displayed corresponds to a single cell. Scale bars, 2 μ m. CTRL: control. Mann-Whitney's tests; *: $p < 0.05$; **: $p < 0.002$; ***: $p < 0.0003$; #: $p > 0.05$.



Appendix Figure-S3 (related to Figure-5D): Quality control of the proteasome inhibitor Epoxomicin (Epo) treatment. HeLa-CIITA cells were treated with Epoxomicin (+) or mock treated (-) for 16h and total ubiquitin levels assessed using Western Blot. The membrane was blotted using an anti-ubiquitin antibody. MW: molecular weight markers.



Appendix Fig S4 (related to Figure-6): Quality controls of T6BP interactome definition. (A) Left panels, gating strategy for the analysis of GFP⁺ cells after transfection of cDNA encoding wild-type T6BP fused to GFP using flow cytometry. FSC: forward scatter; SSC: side-scatter. Right panels, side to side comparison of the percentage of GFP⁺ HeLa-CIITA cells transfected with plasmid encoding GFP-T6BP or GFP-only (pEGFP) in the three biological replicates. **(B)** Coomassie blue staining (left panel) and Western Blot analysis (right panel) of the indicated fraction of protein samples from GFP-T6BP and GFP expressing cells. Results from one of the three biological replicates are shown. Briefly, cells were lysed and submitted to IP using anti-GFP camel antibodies (GFP-Trap from Chromotek). Right panel, GFP and GFP-T6BP were revealed using anti-GFP antibody. FT = Flow through. IP = Immunoprecipitation. **(C)** Coomassie blue staining of immunoprecipitated proteins (1/10 of the sample volume) used for LC-MS/MS analysis (9/10 of the sample volume) of the three biological replicates for both GFP-T6BP and GFP. Due to a mishandling, a crack was unfortunately introduced to the gel when scanning. **(D)** GFP nanobody immunoprecipitates from HeLa-CIITA cells transfected with GFP and T6BP-GFP. 48h post-transfection, IP (IP:GFP) and the total lysate (input) samples were analyzed by Western blot with the indicated antibodies. Input and FT of GFP or T6BP-GFP IP are presented in panel B. **(E)** Silencing of T6BP expression does not influence calnexin (CANX) expression levels. HeLa-CIITA cells transfected with the indicated siRNAs and samples analyzed, 48h post transfection, by Western blot with the indicated antibodies. The ratio of CANX or T6BP expression to actin was quantified using Image J and set at 1 for the control condition.

Appendix Table S1 (related to EV4)

Primers and Probes	Sequence
CD74_S	gAATgCCACCAAgTATggCAA
CD74_R	gggggTCAgCATTCTggA
CD74_P TM	6FAM-CAggTgCATCACATggTCCTCTgT--BBQ
TAX1BP1_L	ggAgTCTTTCCACTggATTAC
TAX1BP1_R	ggCCACATTTTgAAAgATgACA
TAX1BP1_P	6FAM-CCATTgCAgACTTCCAACCTTgCC--BBQ
ACTIN F	AgCCTCgCCTTTgCCgA
ACTIN R	CTggTgCCTggggCg
ACTIN TM	6FAM-CCgCCgCCCgTCCACACCCgCC--BBQ

Reverse transcription quantitative Polymerase Chain Reaction (RT-qPCR) primers: The primers and probes used for quantitation of CD74, T6BP and actin were designed by Olfert Landt and purchased from TIB MolBiol. Sequences are listed in the table below. The RT-qPCRs were performed in a Light Cycler 1.5 instrument in capillaries using a final volume of 20 μ l. The reactions were performed using 300 nM specific sense primer, 300 nM specific antisense primer, 200 nM specific TaqMan probe (TM) and the LightCycler® Multiplex RNA Virus Master mix (ROCHE). The programs were: reverse-transcription 55°C for 10min, initial denaturation 95°C for 5min followed by 45 cycles of amplification. For CD74 and T6BP cycles were: 95°C for 5s, 60°C for 15s + fluorescence measurement and 72°C for 5s. For actin cycles were: 95°C for 20s, 67°C for 30s + fluorescence measurement and 72°C for 5s.